UNIVERSIDADE D
COIMBRA

Tiago Baltazar Félix da Silva

One Dimensional Implementation of a Nonreciprocal and Non-Hermitian Material Response Using Coupled Transmission Lines

Dissertation in the context of the Master of Science in Electrical and Computer Engineering, Specialization in Telecommunications, Subspecialization in Networks and Services and in Wireless and Optical Communications, supervised by Prof. Dr. Tiago André Nogueira Morgado and Prof. Dr. David Emanuel Dias Fernandes and presented to the Faculty of Sciences and Technology, Department of Electrical and Computer Engineering.

February 2023

FCTUC FACULDADE DE CIÊNCIAS
E TECNOLOGIA
UNIVERSIDADE DE COIMBRA

One Dimensional Implementation of a Nonreciprocal and Non-Hermitian Material Response Using Coupled Transmission Lines

Tiago Baltazar Félix da Silva

Coimbra, February 2023

One Dimensional Implementation of a Nonreciprocal and Non-Hermitian Material Response Using Coupled Transmission Lines

Supervisor:

Prof. Dr. Tiago André Nogueira Morgado

Co-Supervisor:

Prof. Dr. David Emanuel Dias Fernandes

Jury:

Prof. Dra. Maria do Carmo Raposo de Medeiros

Prof. Dra. Teresa Martinez dos Santos Gomes

Prof. Dr. Tiago André Nogueira Morgado

Dissertation submitted in partial fulfillment for the degree of Master of Science in Electrical and Computer Engineering.

Coimbra, February 2023

This project was developed with the cooperation of:

Universtity of Coimbra

1 2  9 0

UNIVERSIDADE D
COIMBRA

Electrical and Computing Engineering Department

deer.uc
DEPARTAMENTO DE ENGENHARIA ELETROTÉCNICA
E DE COMPUTADORES

Instituto de Telecomunicações


instituto de
telecomunicações

Acknowledgements

I would like to thank the Instituto de Telecomunicações (IT) - Coimbra and FCT/MCTES for financing in part this work in the framework of the project UIDB/EEA/50008/2020, and for the opportunity and all the conditions given.

My supervisors, Prof. Dr. Tiago Morgado and Prof. Dr. David Fernandes, as well as Dr. Sylvan Lannebère, deserve a particular thank you for their guidance, professionalism, motivation, and constant availability throughout the course of this work. It was a privilege for me to learn and work with you.

I also want to express my gratitude to DEEC/UC, especially the teaching staff, for all the information that was shared and that contributed to mold me into the professional that I am today.

To the NEEEC/AAC, a place that I can still call home, for the amazing two years and for teaching me how to learn from my mistakes, the sense of responsability, and teamwork. To all the people that I met here, paricularly to André, Bento, Diogo, Duarte, Gonçalo, Marta, José Luís, Rafael, among many more.

To my very special friends "Queimados", that stand by me for the past years, for the strength to kept going in the harder times, for the motivation, and for teaching me how to stretch my tongue. To Henriques, Marco, Martins, Moisés, Jorge, and Zé Pedro a very big thank you.

To all the people that had the displeasure to share a house with me and to put up with me, particularly to André, Alexandre, Dinis, Paulo, and more recently Débora.

To my partners in crime Miguel and José for all the debates about football and the NBA, and for mocking with me about the next ones. To my friends "Tarecos" for the company to drink beer and for all the drama that spiced my last months: to Alexandra, António, Carolina Cortez, Carolina Pereira, Catarina, Diogo Cruz, Diogo Felamino, Dora, Margarida, Mário, Moreira, Pedro, and Rita.

To all the people that I met in Coimbra, for all the shared moments. To Carlão, Gonçalo,

Pedro, Rui and Tiago for all the parties in my freshman year. To the guys from Telecom, Guilherme Lemos, Guilherme Lins, José Francisco, José Oliveira, Mário, Óscar and Rafael for all the companionship. I can't forget to thank to Beatriz, Cristiano and José.

Finally, a very special thank you to my parents, my sister and to all my family for the opportunity, the unconditional support and for always believing in me, even when I didn't.

Resumo

Dispositivos não-recíprocos e ativos (com ganho) são de extrema importância em sistemas de microondas e fotónicos. Neste contexto sistemas não-Hermitianos (ou não conservativos) que são sistemas capazes de quebrar a reciprocidade e produzir ganho ótico desempenham um papel crucial.

Nesta dissertação eu desenvolvo e caracterizo, tanto de forma teórica como de forma numérica, um protótipo unidimensional (1D) que opera no regime de microondas do sistema não-recíproco e não-Hermitiano recentemente introduzido, designado de "MOSFET-Metamaterial" (MOSFET-MTM) [1]. Este material hipotético possui propriedades eletromagnéticos únicas permitindo regimes de isolamento ótico e de ganho e/ou perda. A implementação 1D proposta do MOSFET-MTM é baseada em duas linhas de transmissão periodicamente carregadas por transístores FET. A propagação das ondas nas linhas de transmissão acopladas é caracterizada, tanto teoricamente como numericamente e é demonstrado que possibilita fortes respostas não-reciprocas e não-Hermitianas. Nos estudos teóricos, considerei dois modelos distintos: um em que as linhas periodicamente carregadas são estudadas como um meio efetivo com parâmetros distribuídos (modelo do meio efetivo) e outro que tem em consideração a granularidade da estrutura. É mostrado que desde que se garanta que a distância entre FETs consecutivos seja muito menor que o comprimento de onda da radiação, o modelo efetivo mais simples pode ser utilizado de forma fiel para caracterizar a propagação nas linhas acopladas. Numa fase inicial, eu considero um sistema formado por FETs ideais que são caracterizados por um circuito sem elementos extrínsecos (parasitas) e em que a capacitância *gate-to-drain* é desprezada ($C_{gd} = 0$), tal que os FETs se comportam como dispositivos unidirecionais ideais. Depois, eu analiso a resposta do sistema usando FETs mais realistas com $C_{gd} \neq 0$ e tendo em conta os elementos parasitas. Além disso, os resultados teóricos são validados com simulações numéricas com recurso ao *software* comercialmente disponível ADS [2]. Finalmente, para ser capaz caracterizar experimentalmente o proposto MOSFET-MTM 1D, atualmente está a ser fabricado um protótipo de microondas

com base em técnicas comuns de impressão de circuitos.

Os resultados teóricos e numéricos demonstram que a estrutura 1D análoga do MOSFET-MTM proposta possui fortes respostas não-recíproca e com ganho ou perdas (ou seja, resposta não-Hermitiana).

Abstract

Nonreciprocal and active (with gain) devices are of uttermost importance in microwave and photonic systems. Non-Hermitian (or energy non-conserving) systems capable of breaking nonreciprocity and produce optical gain play a crucial role in such context.

Here I develop and characterize, both theoretically and numerically, a 1-dimensional (1D) prototype operating in the microwave regime of the recently introduced nonreciprocal and non-Hermitian system designated as "MOSFET-Metamaterial" (MOSFET-MTM) [1]. This idealized material possesses unique electromagnetic properties and enables regimes of optical isolation and gain/loss. The proposed 1D implementation of the MOSFET-MTM is based on two coupled transmission lines periodically loaded with FET transistors. The wave propagation in the coupled transmission lines is characterized both theoretically and numerically and it is demonstrated that the proposed structure enables strong nonreciprocal and non-Hermitian responses. In the theoretical studies, I considered two distinct models: one where the periodically loaded lines are regarded as a continuous medium with distributed parameters (effective medium model) and another that takes into account all the granular details of the structure. It is shown that provided the distance between consecutive FETs is much smaller than the wavelength of the radiation the simpler effective medium model can be accurately used to characterize the wave propagation in the coupled lines. At a first stage, I consider a system formed by ideal FETs characterized by circuits without extrinsic (parasitic) elements and in which the gate-to-drain capacitance ($C_{gd} = 0$) is neglected, so that the FETs behave as truly unidirectional devices. After that, I analyze the response of the system using more realistic FETs with $C_{gd} \neq 0$ and taking into account the parasitic elements. Furthermore, the theoretical results are validated with numerical simulations using the commercially available software ADS [2]. Finally, in order to be able to experimentally characterize the proposed 1D MOSFET-MTM, a microwave prototype is currently being fabricated using standard printed circuits techniques.

The theoretical and numerical results demonstrate that the proposed 1D analog of the

MOSFET-MTM enables strong nonreciprocal responses of gain or loss (i.e., non-Hermitian response).

Keywords

MOSFET-Metamaterial, Nonreciprocity, Non-Hermititan Systems, Coupled Transmission Lines, FET Isolators.

“You should always discuss the defeats because you can learn much more from failure than from success."

— Niki Lauda

“Every day is a new adventure."

— Stan Lee

Contents

List of Acronyms

1D	1-Dimensional
ADS	Advanced Design System
FET	Field-Effect Transistor
MESFET	Metal-Semiconductor Field-Effect Transistor
MOSFET	Metal-Oxide-Semiconductor Field-Effect Transistor
MTM	Metamaterial
PCB	Printed Circuit Board
p.u.l.	per unit of length
SMA	SubMiniature version A
SMD	Surface-mount Device
TL	Transmission Line
TR	Time-Reversal
VNA	Vector Network Analyzer

List of Figures

List of Tables

1 Introduction

1.1 Context and Motivation

In typical linear, time-invariant, and passive microwave and photonic systems, the wave propagation is restricted by the Lorentz reciprocity law [3]. According to the Lorentz reciprocity principle, in reciprocal systems the level of transmission between two points is the same independent of the propagation direction. In other words, this means that wave propagation in reciprocal systems is intrinsically bidirectional.

However, breaking reciprocity and obtaining nonreciprocal devices, such as isolators and circulators, is fundamental in many telecommunications systems and networks. In general, to achieve nonreciprocal electromagnetic responses we need to either (i) break time-reversal (TR) symmetry with an external bias, or (ii) use nonlinear materials, or (iii) exploit non-Hermitian physics. The most common way to break the TR symmetry and obtain strong nonreciprocal responses is by using magneto-optical materials (such as ferrites) biased with a static magnetic field [3]. However, the requirement of having an external biasing circuit poses an important barrier to incorporating these solutions in microwave and photonic integrated circuits. Due to this, several non-magnetic nonreciprocal solutions with broken TR symmetry that can be integrated into on-chip circuits have been proposed. These include systems with time-modulated parameters [6, 7], active electronic solutions [8], systems with drifting electrons [9], etc. Alternatively, nonreciprocal responses can be obtained with nonlinear dynamic systems [10, 11].

Another possibility to break reciprocity is offered by non-Hermitian systems. A system with non-Hermitian response is not bound by energy conservation [12–15] so that it can either have loss or gain. In non-Hermitian systems the constitutive parameters are not bound by the relations $\bar{\varepsilon} = \bar{\varepsilon}^{\dagger}$ and $\bar{\mu} = \bar{\mu}^{\dagger}$ (the superscript † represents the operation of transpose-conjugation) as in usual energy conserving systems. Moreover, exploiting non-Hermitian physics to obtain nonreciprocity can allow for very unique responses. In particular, inspired

by the physics of transistors, it was recently proposed in [1] a new mechanism for creating a material with a strong nonreciprocal and non-Hermitian (non-conservative) response. It was theoretically demonstrated in [1] that a hypothetical bulk metamaterial formed by a periodic arrangement of MOSFETs (designated as "MOSFET-metamaterial") [see Fig.1.1b] could behave as either a lossy (i.e, absorbs energy) or a gainy (i.e, behaves as an amplifier) material, depending on the field polarization. Moreover, it was shown that it can be used to realize an electromagnetic isolator whose performance may surpass that of standard Faraday isolators.

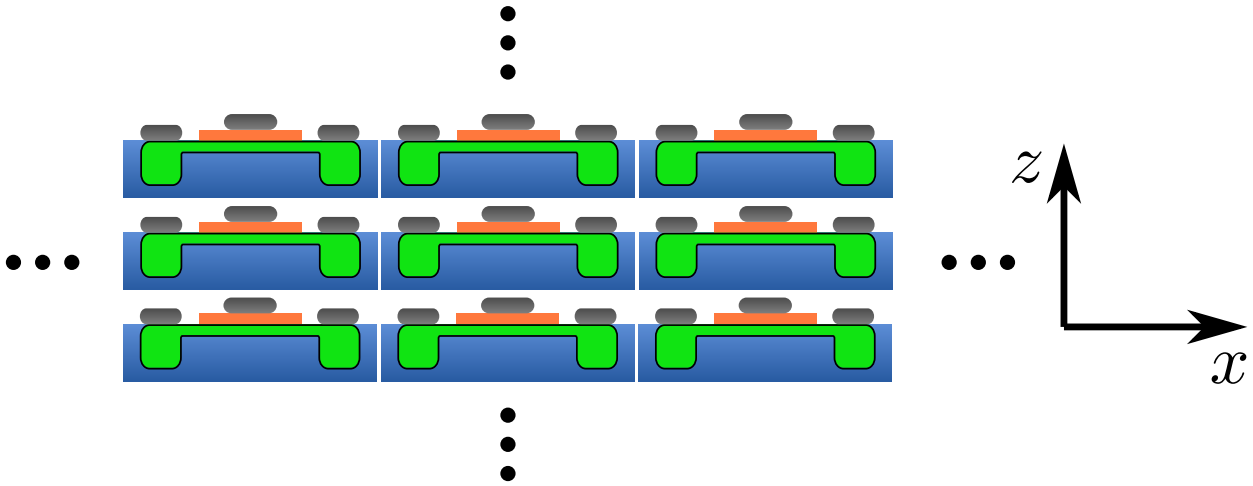

Figure 1.1: Sketch of the MOSFET-Metamaterial formed by a periodic array of MOSFETs transistors. *Adapted from [1].*

1.2 Main Goals of this Dissertation

The main goal of this dissertation is the implementation of a 1D analog of the MOSFET-metamaterial proposed in [1] based on transmission line (TL) technology operating at microwave frequencies. The idea is to use a system formed by two microstrip TLs periodically loaded with FET isolators [see Fig. 1.2].

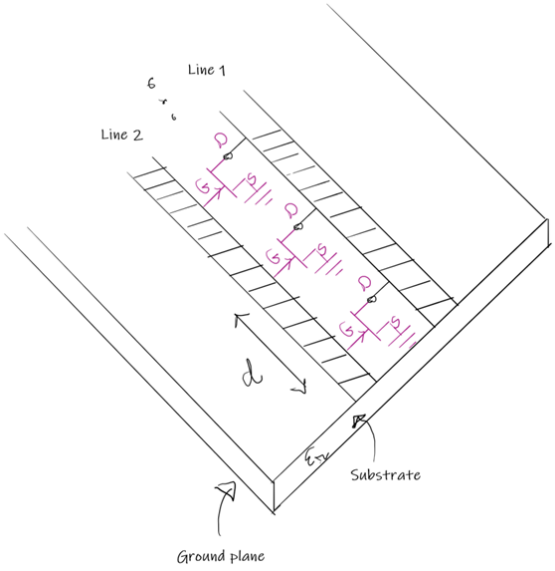

Figure 1.2: 1D implementation of the MOSFET-MTM: two microstrips lines periodically coupled with FET isolators.

The proposed system will be studied theoretically and numerically to demonstrate that it can enable strong nonreciprocal responses and regimes of gain and loss (i.e., that it has a non-Hermitian response). Furthermore, a prototype of the studied configuration is proposed to experimentally demonstrate the non-Hermitian and nonreciprocal response of the 1D analog of the MOSFET-MTM.

1.3 Dissertation Outline

The remaining structure of this dissertation contains three more chapters. In Chapter 2, will be presented the main electromagnetic properties of the MOSFET-MTM and the consequences of the wave propagation in the metamaterial, more specifically the *power beating* and the possibility of obtaining an optical isolator. In Chapter 3, it will be presented the analog 1D structure of the MOSFET-MTM, which will be based on TL periodically coupled with FET isolators. Firstly it is explained the analogy between the wave propagation in the coupled lines and in the MOSFET-MTM. Afterward, it is explained how the FET isolator response is modeled and incorporated into the theoretical model. To theoretically study the wave propagation in the TL I consider two distinct models. In the first model the FET parameters are distributed along the line and the system is regarded as a continuous medium. In the second model, the periodic loading of the lines is explicitly taken into account. Both models are validated against full wave simulations calculated using ADS [2]. Finally, the the-

oretical and numerical simulations are used to design a microwave prototype based on PCB technology and commercially available elements. In the last chapter, the main conclusions of the work are outlined, as well as the future work.

2 MOSFET-Metamaterial

2.1 Nonreciprocal and Non-Hermitian Response in the MOSFET-Metamaterial

In Ref. [1], it was introduced a hypothetical bulk metamaterial, designated as MOSFET-Metamaterial, composed by a periodic arrangement of MOSFET transistors [see Fig. 1.1b]. It was theoretically demonstrated in [1] that when such hypothetical metamaterial is biased with some static electric field $\mathbf{E}^0$ in the xoz plane, for dynamic fields ($\mathbf{E}^\omega$) with small amplitude compared to $\mathbf{E}^0$ $\left(\text{i.e., } |\mathbf{E}^\omega| << \left|\mathbf{E}^0\right|\right)$, the electromagnetic response is described by the following linearized permittivity tensor:

$$\bar{\varepsilon} = \begin{bmatrix} \varepsilon_{xx} & 0 & \varepsilon_{xz} \\ 0 & \varepsilon_{yy} & 0 \\ 0 & 0 & \varepsilon_{zz} \end{bmatrix}. \tag{2.1}$$

Interestingly, this linearized permittivity tensor indicates that the electromagnetic response of the MOSFET-MTM is nonreciprocal $\left(\bar{\varepsilon}^T \neq \bar{\varepsilon}\right)$ (the superscript ^{T} represents the operation of transpose), and non-Hermitian $\left(\bar{\varepsilon}^\dagger \neq \bar{\varepsilon}\right)$. Therefore, this permittivity tensor predicts that the MOSFET-MTM may exhibit quite remarkable properties. The propagation along the $y-$direction ($\nabla = \partial_y \hat{\mathbf{y}}$) can be described by the expanded form of Maxwell's equations:

$$-j\partial_y E_x = \omega\mu_0 H_z, \qquad j\partial_y E_z = \omega\mu_0 H_x \tag{2.2a}$$

$$j\partial_y H_x = \omega\varepsilon_0\varepsilon_{zz} E_z, \qquad -j\partial_y H_z = \omega\varepsilon_0 \left(\varepsilon_{xx} E_x + \varepsilon_{xz} E_z\right) \tag{2.2b}$$

where is considered a time variation $e^{j\omega t}$ and $\partial_y = \partial/\partial y$.

The wave propagation in the MOSFET-MTM is characterized by $\nabla \times \nabla \times \mathbf{E} = (\omega^2/c^2)\,\bar{\varepsilon} \cdot \mathbf{E}$, where ω is the angular frequency and c the speed of light in vacuum. The plane wave

solutions are of the form $\mathbf{E} = \mathbf{A}_0 e^{-j\mathbf{k}\cdot\mathbf{r}}$ with $\mathbf{A}_0$ a constant complex vector, $\mathbf{k}$ the wave vector and $\mathbf{r} = x\hat{\mathbf{x}} + y\hat{\mathbf{y}} + z\hat{\mathbf{z}}$ the position vector. For propagation along the $y-$direction, the solutions of the homogeneous wave equation are:

$$\mathbf{k} = \frac{\omega}{c}\sqrt{\varepsilon_{xx}}\hat{\mathbf{y}} \equiv \mathbf{k}_o, \quad \mathbf{E}\sim\hat{\mathbf{x}} \qquad \text{(ordinary wave)} \tag{2.3a}$$

$$\mathbf{k} = \frac{\omega}{c}\sqrt{\varepsilon_{zz}}\hat{\mathbf{y}} \equiv \mathbf{k}_e, \quad \mathbf{E}\sim\frac{\varepsilon_{xz}}{\varepsilon_{zz}-\varepsilon_{xx}}\hat{\mathbf{x}} + \hat{\mathbf{z}} \qquad \text{(extraordinary wave).} \tag{2.3b}$$

Notably, because of the non-Hermitian response stemming from the nonzero cross-coupling coefficient ε_{xz}, the two wave modes are non-orthogonal [see Fig. 2.1]. In particular, the electric field vector of the extraordinary wave makes an angle θ (with $\tan(\theta) = (\varepsilon_{xz}/(\varepsilon_{zz}-\varepsilon_{xx}))$) with the direction perpendicular to the electric field vector of the ordinary mode. It is important to note that in conventional lossless and Hermitian materials, the electromagnetic modes are always orthogonal. As shown in the next section, the nonorthogonality of the two electromagnetic modes may lead to interesting effects and opportunities.

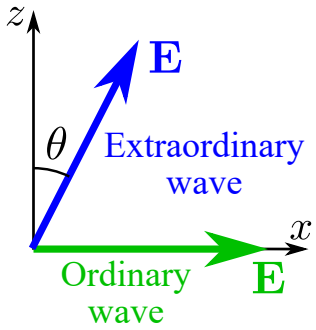

Figure 2.1: Geometrical relation between the electrical field of the plane wave modes in the MOSFET-MTM [Eq. 2.3] for propagation along y. *Adapted from [1].*

2.2 Power Flow in the MOSFET-Metamaterial

Assuming a superposition of the two waves (ordinary and extraordinary), it can be shown [1] that the time-averaged Poyting vector $\mathbf{S} = \frac{1}{2}\mathrm{Re}\{\mathbf{E}\times\mathbf{H}^*\}$ in the material is given by:

$$\mathbf{S} = \frac{1}{2}\frac{\sqrt{\varepsilon_0}}{\sqrt{\mu_0}}\left[|A_o|^2\sqrt{\varepsilon_{xx}} + |A_e|^2\sqrt{\varepsilon_{zz}}\left(1+\left|\frac{\varepsilon_{xz}}{\varepsilon_{zz}-\varepsilon_{xx}}\right|^2\right) + \frac{1}{\sqrt{\varepsilon_{zz}}-\sqrt{\varepsilon}_{xx}}\mathrm{Re}\left\{\varepsilon_{xz}A_eA_o^*e^{-j(k_e-k_o)y}\right\}\right]\hat{\mathbf{y}} \tag{2.4}$$

The first two terms of $\mathbf{S}$ represent the power transported by the two waves (ordinary and extraordinary) individually. Remarkably, provided the cross-coupling coefficient ε_{xz} is

different from zero, there is a third term that is responsible for a periodic spatial variation of the power flux. This third term describes a *power beating* with spatial frequency $k_e - k_o$, as illustrated in Fig. 2.2. Therefore, when $\varepsilon_{xz} \neq 0$, the two modes cease to transport the power independently in the material. This is a very unusual result since in standard Hermitian systems the electromagnetic modes always transport power independently.

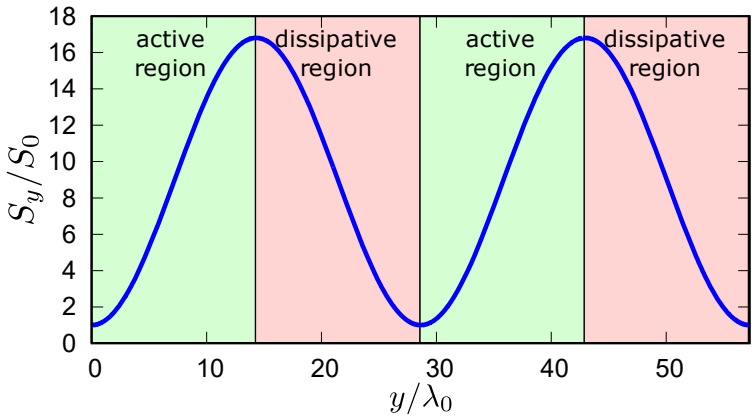

Figure 2.2: Poyting vector (normalized) as a function of the propagation distance (normalized to the vacuum wavelength $\lambda_0 = 2\pi c/\omega$). *Adapted from [1].*

As one can see from Fig. 2.2, depending on the phase between the ordinary and extraordinary waves, the MOSFET-MTM alternates between active and dissipative regions. The level of power amplification is proportional to the magnitude of the cross-coupling component ε_{xz}.

2.3 MOSFET-Metamaterial as an Electromagnetic Isolator

As already pointed out, an interesting property of the MOSFET-MTM is that the eigenvectors of the ordinary and extraordinary waves are not orthogonal. As theoretically demonstrated in [1], this property can be exploited to design an electromagnetic isolator, as depicted in Fig. 2.3. The isolator consists of a MOSFET-MTM slab of thickness d placed in between two orthogonal linear polarizers. The purpose of the two linear polarizers is to absorb the electric field component parallel to their axes, and let the orthogonal components pass them unaltered.

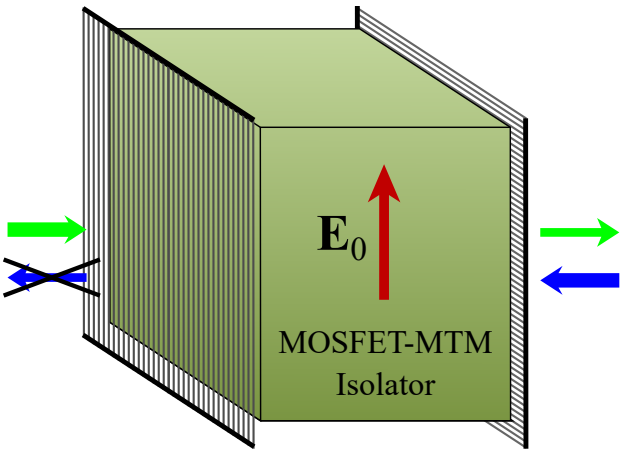

Figure 2.3: Electromagnetic isolator based on the electrically biased MOSFET-MTM. *Adapted from [1].*

Let us analyze the response of such an isolator. One can see that for an incident wave that propagates in the positive y direction (from left to right), the polarizing grid absorbs its x component, i.e., the wave reaching the MOSFET-MTM slab only has electric field oriented along the $z-$direction. But, because of the cross-coupling term ε_{xz}, the wave propagation in the metamaterial may induce an electrical field component along x, generating an output signal from left to right. On the other hand, an incident wave propagating from right to left can only enter into the metamaterial if the incident electric field has an electric field component along x. In this scenario, the MOSFET-MTM does not generate any cross-polarization component, so the incoming wave is totally absorbed by the grid, and hence, there is no right-to-left transmission. Therefore, the system behaves as an isolator, since the wave propagation is only allowed in a specific (left to right) direction.

3 1D Implementation of the MOSFET-MTM using asymmetrically coupled TL

In the previous chapter, I introduced the MOSFET-MTM, a hypothetical material that draws inspiration from standard MOSFETs and possesses unique electromagnetic properties such as a nonreciprocal and non-Hermitian responses. The remarkable properties of the MOSFET-MTM can allow for exotic wave phenomena such as a *power beating* characteristic and permitting realizing optical isolators in magneteless systems. In this chapter, I purpose a 1D implementation of such a hypothetical material. The proposed configuration is based on two coupled transmission lines periodically loaded with FET isolators. I explore the unique wave phenomena that this structure can produce and demonstrate that it can indeed behave as a 1D version of the MOSFET-MTM.

3.1 Coupled TL Analogy

The main motivation to use a coupled TL structure to mimic the MOSFET-MTM response is related to the fact that the equations that determine the electromagnetic field in the MOSFET-MTM are very similar to the standard equations that describe the wave propagation in capacitively coupled TL configuration [3].

Let's start by considering a system consisting of two capacitively coupled transmission lines (TL) oriented along $y-$direction. The wave propagation in this structure can be determined using:

$$j\partial_y V_1 = \omega L_{11} I_1 \tag{3.1a}$$

$$j\partial_y I_1 = \omega \left(C_{11} V_1 + C_{12} V_2\right) \tag{3.1b}$$

$$j\partial_y V_2 = \omega L_{22} I_2 \tag{3.1c}$$

$$j\partial_y I_2 = \omega \left(C_{21} V_1 + C_{22} V_2\right), \tag{3.1d}$$

The coupling between the two lines is described by the mutual capacitances (per unit of length) C_{12} and C_{21}.

In reciprocal systems, the mutual capacitances are identical such as $C_{12} = C_{21} \equiv C_m$ [see Fig. 3.1a]. Here, on the other hand, to mimic the response of the MOSFET-MTM I consider a more exotic response such that the lines are asymmetrically coupled with $C_{12} \neq 0$ and $C_{21} = 0$ [see Fig. 3.1b]. This type of capacitive coupling causes the voltages and currents in line 1 to be influenced by the wave propagating in line 2, but line 2 is insensitive to the voltages and currents of the wave propagating in line 1.

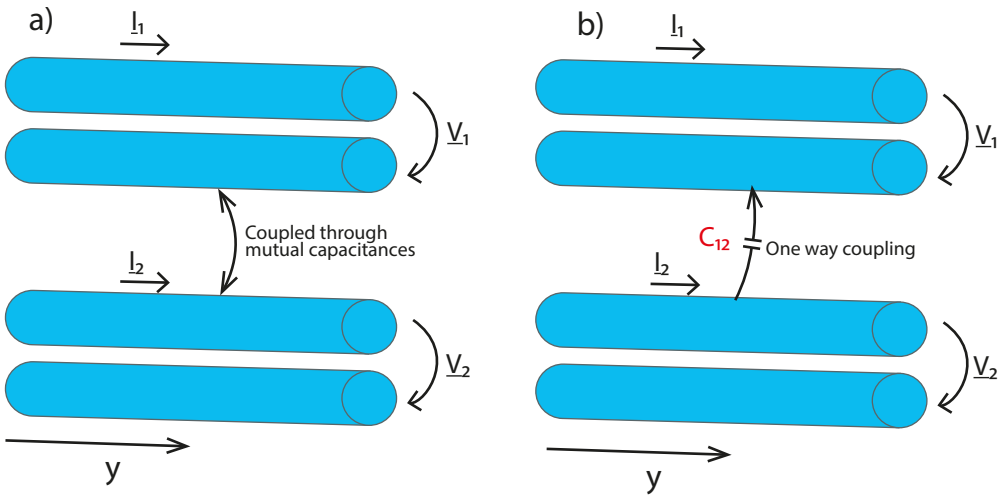

Figure 3.1: a) Two transmission lines are capacitively coupled, with $C_{12} = C_{21} \equiv C_m$. b) Two transmission lines coupled through a one-way capacitance p.u.l. such that $C_{12} \neq 0$ and $C_{21} = 0$.

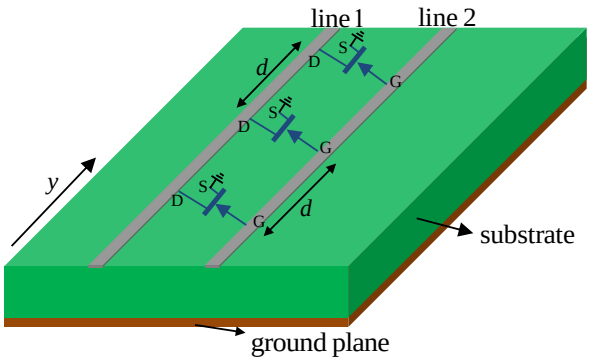

Figure 3.2: Two microstrips TL periodically loaded with FET isolators

To implement the asymmetrically coupled lines in a real physical system I consider two TL periodically loaded with FET isolators (with period d) as illustrated in Fig. 3.2. Here, it is adopted a common-source FET configuration [see Fig. 3.3], with the source connected to

the ground plane. In a common-source configuration the FETs may be regarded as a 2-port device with the small-signal equivalent circuit depicted in Fig. 3.4.

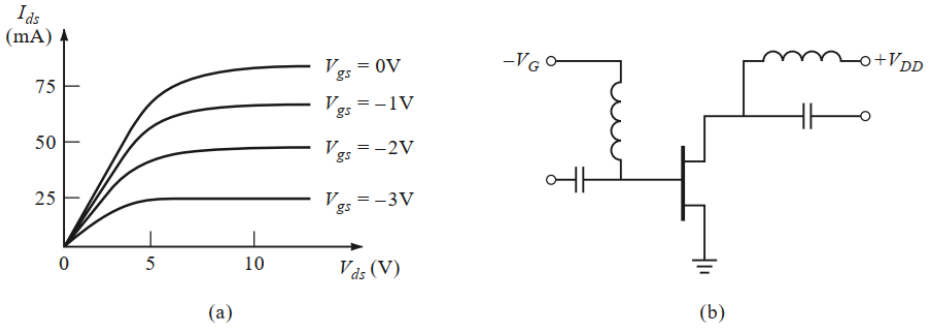

Figure 3.3: Common-source configuration for a depletion mode MESFET. *Adapted from [3].*

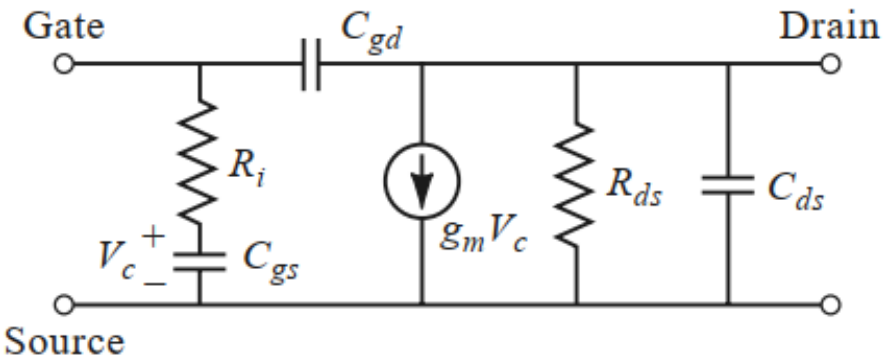

Figure 3.4: Small signal equivalent for a microwave FET in common-source configuration. *Adapted from [3].*

This equivalent circuit is the result of a linearization of the FET response around the operation point.

In what follows it is described how the FET model is incorporated into the analysis of the system. The FET elements can be modeled by an admittance matrix $\mathbf{Y}_{\mathrm{F}}$, which relates the currents and voltages at the two ports as:

$$\begin{bmatrix} I_{m1} \\ I_{m2} \end{bmatrix} = \begin{bmatrix} Y_{11} & Y_{12} \\ Y_{21} & Y_{22} \end{bmatrix} \begin{bmatrix} V_{m1} \\ V_{m2} \end{bmatrix}. \tag{3.2}$$

Lets start by obtaining an equivalent continuous model for the circuit in Fig. 3.2 in which the FET parameters are distributed along the line. The model is valid under the metamaterial regime, i.e., when the spacing d between sucessive FETs is much smaller than the wavelength in the TL [16].

Importantly, when the FETs are connected to the TLs there is a discontinuity of the currents in the two lines at the connection points. However, the voltages remain continuous at those points. Thus, in the effective medium regime $\mathbf{Y}_{\mathrm{F}}$ will contribute to the distributed capacitance of the lines. Indeed, the additional capacitance p.u.l. is $\mathbf{Y}_{\mathrm{F}}/(j\omega d)$. Hence, the effective capacitances of the periodically loaded system are:

$$C_{11} = C_1 + \frac{\mathbf{Y}_{\mathrm{F},11}}{j\omega d}, \qquad C_{12} = \frac{\mathbf{Y}_{\mathrm{F},12}}{j\omega d}, \tag{3.3a}$$

$$C_{21} = \frac{\mathbf{Y}_{\mathrm{F},21}}{j\omega d}, \qquad C_{22} = C_2 + \frac{\mathbf{Y}_{\mathrm{F},22}}{j\omega d}. \tag{3.3b}$$

C_1 and C_2 are the capacitances p.u.l. of the unloaded microstrip lines (i.e., the lines without the FETs). Note that the effective inductances are the same as for the uncoupled lines, i.e., the inductances are unaffected by the loading of the FETs.

3.2 Admittance matrix of the FET

Here it is described how the admittance matrix $\mathbf{Y}_{\mathrm{F}}$ that describes the response of the FET isolator is calculated. To begin with, as described in [3] the small gate-to-drain capacitance (C_{gd}) of the equivalent circuit shown in Fig. 3.4 is neglected. The corresponding small-signal equivalent circuit of the FET is depicted in Fig. 3.5.

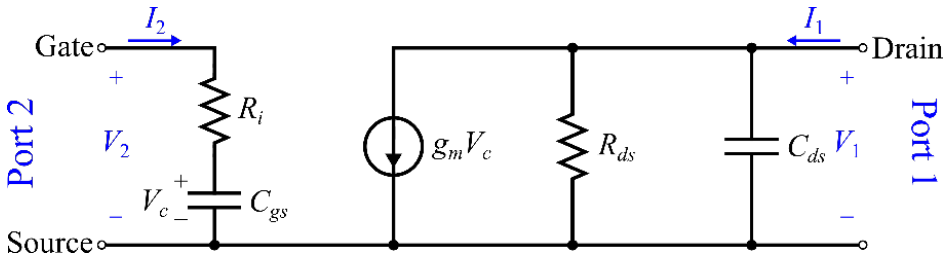

Figure 3.5: Small signal equivalent circuit for a microwave FET in common-source configuration with the small gate-to-drain capacitance (C_{gd}) neglected.

A simple analysis of this circuit shows us that the admittance matrix is given by:

$$\mathbf{Y}_{\mathrm{F}} = \begin{bmatrix} \frac{1}{R_{ds}} + j\omega C_{ds} & g_m \frac{1}{1+j\omega C_{gs} R_i} \\ 0 & \frac{j\omega C_{gs}}{1+j\omega C_{gs} R_i} \end{bmatrix}. \tag{3.4}$$

Note that $\mathbf{Y}_{\mathrm{F},21} \approx 0$, and thereby, the FET isolator is strictly unidirectional, which leads to $C_{21} = \frac{\mathbf{Y}_{\mathrm{F}21}}{j\omega d} \approx 0$. To avoid insertion losses, we, ideally, would like to have $\omega C_{ds} R_{ds} >> 1$ and $\omega C_{gs} R_i << 1$. The first condition can be met by having a large R_{ds}, which can be

obtained by operating the FET in the saturation region [see Fig. 3.3] wherein the drain to source current I_{ds} is insensible to variations of V_{ds}. The second condition is obtained by having the smallest losses possible such that $R_i = 0$. Under these conditions, the admittance matrix simplifies and is given by:

$$\mathbf{Y}_{\mathrm{F}} = \begin{bmatrix} j\omega C_{ds} & g_m \\ 0 & j\omega C_{gs} \end{bmatrix}, \tag{3.5}$$

and we can obtain the following effective capacitance:

$$C_{ef} = \begin{bmatrix} C_{11} & C_{12} \\ C_{21} & C_{22} \end{bmatrix} \approx \begin{bmatrix} C_1 + \frac{C_{ds}}{d} & \frac{g_m}{j\omega d} \\ 0 & C_2 + \frac{C_{gs}}{d} \end{bmatrix}. \tag{3.6}$$

While the effective inductance is given by:

$$\mathbf{L}_{ef} = \begin{bmatrix} L_{11} & 0 \\ 0 & L_{22} \end{bmatrix}. \tag{3.7}$$

In Eq. 3.6 is shown that the effective response of the coupled lines is very identical to the response of the MOSFET-MTM. However, the capacitance C_{12} is purely imaginary, while the corresponding cross-coupling coefficient ε_{xz} in the MOSFET-MTM is real.

3.3 Wave Propagation in the Asymmetrically Coupled TL

3.3.1 Effective or distributed parameters model

The wave propagation in the capacitively coupled lines is determined by solving the linear equations 3.1, considering the effective capacitive and inductive elements that are given by Eqs. 3.6 and 3.7, respectively. So it can be rewriten the Eqs. 3.1 in a compact format like $j\partial_y \mathbf{f} = \mathbf{M} \cdot \mathbf{f}$, with the matrix $\mathbf{M}$ given by:

$$\mathbf{M} = \omega \begin{bmatrix} 0 & 0 & L_{11} & 0 \\ 0 & 0 & 0 & L_{22} \\ C_{ef,11} & C_{ef,12} & 0 & 0 \\ 0 & C_{ef,22} & 0 & 0 \end{bmatrix}, \tag{3.8}$$

with $\mathbf{f} = (V_1, V_2, I_1, I_2)^T$, the state vector formed by the voltages and the currents in the two microstrip lines. The traveling wave solutions, with a spatial variation in y of the form

$e^{-jk_y y}$, can be found in a very direct way from the kernel of the matrix $\mathbf{M}$. Analogous to the MOSFET-MTM, there are two traveling waves, an ordinary and an extraordinary wave. The ordinary wave is of the form:

$$\mathbf{f}_o = \begin{bmatrix} \mathbf{V}_o \\ \mathbf{I}_o \end{bmatrix} = A_o \begin{bmatrix} \sqrt{\frac{L_{11}}{C_{11}}} \\ 0 \\ 1 \\ 0 \end{bmatrix} e^{-j\beta_o y}, \text{ with } \beta_o = \omega\sqrt{L_{11}C_{11}} \tag{3.9}$$

where A_o is the complex amplitude of the wave and with $\mathbf{V}_o$ and $\mathbf{I}_o$ the vectors with the two components of the voltages and currents, respectively. The ordinary wave describes a wave that solely propagates in line 1. Recall that line 2 is totally insensitive to the distribution of voltages and currents in line 1. On the other side, the extraordinary wave mode describes a wave that propagates in line 2 and that will leak its energy into line 1, due to the one-way coupling that is provided by the FET isolators, with its corresponding state vector being given by:

$$\mathbf{f}_e = \begin{bmatrix} \mathbf{V}_e \\ \mathbf{I}_e \end{bmatrix} = A_e \begin{bmatrix} \sqrt{\frac{L_{22}}{C_{22}}} \frac{C_{12}L_{11}}{C_{22}L_{22}-C_{11}L_{11}} \\ \sqrt{\frac{L_{22}}{C_{22}}} \\ \frac{C_{12}L_{11}}{C_{22}L_{22}-C_{C_{11}L_{11}}} \\ 1 \end{bmatrix} e^{-j\beta_e y}, \text{ with } \beta_e = \omega\sqrt{L_{22}C_{22}} \tag{3.10}$$

where A_e is the complex amplitude of the extraordinary wave mode.

The total power flowing in two lines can be given by the product of the voltages and the currents in both lines as:

$$P = \frac{1}{2}\mathrm{Re}\left\{V_1 I_1^* + V_2 I_2^*\right\} = \frac{1}{2}\mathrm{Re}\left\{\mathbf{V}\cdot\mathbf{I}^*\right\} \tag{3.11}$$

with $\mathbf{V} = \begin{bmatrix} V_1 \\ V_2 \end{bmatrix}$ and $\mathbf{I} = \begin{bmatrix} I_1 \\ I_2 \end{bmatrix}$. A standard solution of $j\partial_y \mathbf{f} = \mathbf{M}\cdot\mathbf{f}$ may be written as a superposition of the two eigenwaves supported by the lines. Hence, the power distribution in all space may also be written as a function of a generic solution (superposition of the two eigenmodes) of the system and is given by

$$P = \frac{1}{2}\mathrm{Re}\left\{\mathbf{V}_o\cdot\mathbf{I}_o^*\right\} + \frac{1}{2}\mathrm{Re}\left\{\mathbf{V}_e\cdot\mathbf{I}_e^*\right\} + \frac{1}{2}\mathrm{Re}\left\{\mathbf{V}_e\cdot\mathbf{I}_o^* + \mathbf{V}_o\cdot\mathbf{I}_e^*\right\} = \mathbf{P}_o + \mathbf{P}_e + \mathbf{P}_{cr} \tag{3.12}$$

where $\mathbf{P}_o$ and $\mathbf{P}_e$ are the powers transported by the ordinary and extraordinary waves alone, and $\mathbf{P}_{cr}$ is an interference term.

As shown in Eq. 3.12 the power distribution in the lines contains one interference term resulting from the interaction between the ordinary and extraordinary waves that originate from the unidirectional coupling from line 2 to line 1. This interference term can cause the emergence of a *power beating*. The capacitances and inductances p.u.l. of the unloaded lines can be given by:

$$C_i = \frac{1}{Z_{0,i}\nu_{p,i}}, \qquad L_i = \frac{Z_{0,i}}{\nu_{p,i}}, \tag{3.13}$$

with $\nu_{p,i} = c/\sqrt{\varepsilon_{ef,i}}$ the velocity of propagation in the i-th line. Moreover, we consider a FET transistor with parameters given by table 3.1, taken from [3].

Table 3.1: Typical values for the equivalent circuit of microwave MESFET [3].

Parameter	**Value**
R_i (series gate resistance)	7Ω
R_{ds} (drain-to-source resistance)	400Ω
C_{gs} (gate-to-source capacitance)	0.3pF
C_{ds} (drain-to-source capacitance)	0.12pF
g_m (transconductance)	40mS

The distance between two adjacent transistors, i.e., the spatial period, is assumed to be $d = 5$mm. It is also considered that line 1 is shorted-circuited at $y = 0$ so that $V_1(y = 0) = 0$. In this scenario, it is easily shown that for these conditions to be satisfied, in a generic solution of the system 3.1 the complex amplitude of the ordinary and extraordinary wave modes (A_o and A_e, respectively) must satisfy:

$$A_o = -A_e \cdot \sqrt{\frac{C_{11}}{L_{11}}}\sqrt{\frac{L_{22}}{C_{22}}}\frac{C_{12}L_{11}}{C_{22}L_{22} - C_{11}L_{11}}. \tag{3.14}$$

In this initial stage, the dissipative elements of the FET equivalent circuit are ignored, and it is supposed that $R_i = 0$ and $R_{ds} = \infty$. In Fig. 3.6, it is depicted the spatial distribution of the voltage and current in the two TL for a fixed frequency of operation $\omega/(2\pi) = 5$GHz. In the horizontal axis is depicted the propagation distance in terms of the number of unit cells present in the system. Figure 3.6 shows us that the voltage and current in line 2 has a constant value, because, as previously mentioned, the waves in this line are insensitive to the wave in line 1. On the other hand, the voltage and current in line 1 have a periodic variation in space, because of the interference between the ordinary and extraordinary waves.

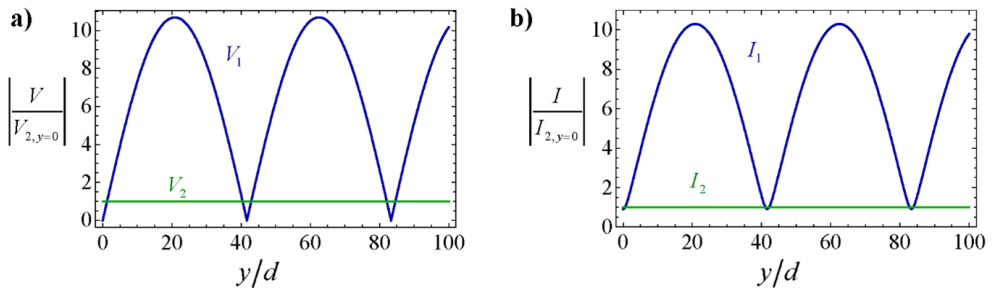

Figure 3.6: Spatial distribution of the voltage [a)] and current [b)] in the coupled TL as a function of the propagation distance.

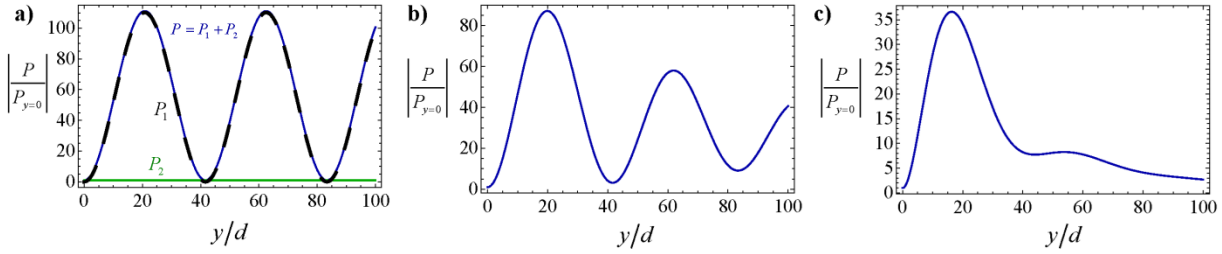

Figure 3.7: Total power transported by the two lines as a function of the propagation distance (blue lines). a) Ideal scenario where the FET isolators have $R_i = 0$ and $R_{ds} = \infty$ and individual powers transported by line 1 (dashed black line) and line 2 (green line). b) FET isolators with $R_i = 7\Omega$ and $R_{ds} = \infty$. c) FET isolators with $R_i = 7\Omega$ and $R_{ds} = 400\Omega$ [see Table 3.1].

When the influence of the dissipative elements (R_i and R_{ds}) is discarded [see Fig. 3.7a], the power flows periodically with the propagation distance with a period of roughly $40d$ (i.e., every 40 transistors). In Fig. 3.7a it is shown that due to the gain of the transistors, the total power of the system can exceed more than 100 times the input power. Also it is possible to see that in some regions the FETs transistors pump energy into the system (increasing the transported power). And in other regions, the FETs transistors extract energy from the system (decreasing the transported power). This gives rises to the effect of the *power beating*. Fig. 3.7 also shows that most of the energy is transported in line 1 (dashed black line), and there isn't any power oscillation in line 2 (green line).

Interestingly, when some of the dissipative elements of the FET are taken into account (R_i), it is possible to see that the power oscillations are damped after a few periods of signal [see Fig. 3.7b]. On the other hand when all of those elements (R_i and R_{ds}) are considered, the power oscillations are damped after the first period of signal [see Fig. 3.7c].

3.3.2 Discrete model

Until this point, all theoretical calculations were performed considering that the FET parameters were distributed along the periodically loaded TLs [see Fig. 3.2]. However, such model may break its validity when the spacing between FETs is on the order or larger of the wavelength of radiation. In what follows, I develop a theoretical model in which the FET is considered a punctual load and I modulate its behave based on that effect.

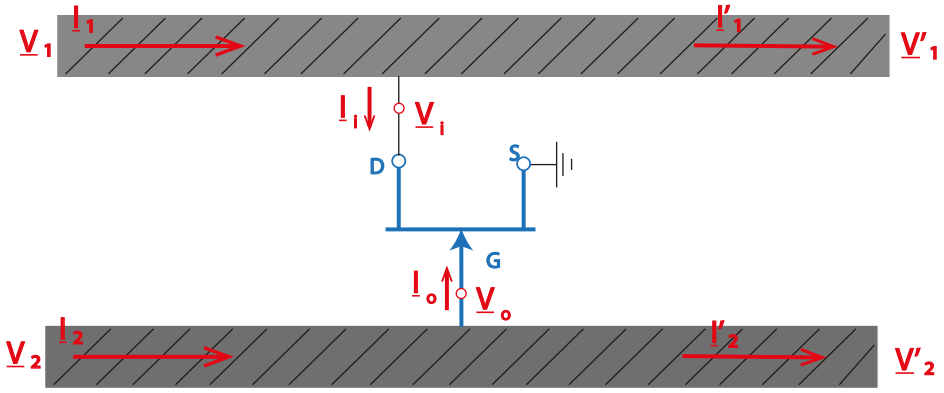

Figure 3.8: Sketch of the connection of the TL through a FET isolator.

The model is based on a transfer matrix (ABCD matrix) formalism that takes into account exactly the periodicity of the system. To begin with, I obtain the equivalent ABCD matrix $\mathbf{T}$ for a FET isolator. This matrix relates the voltage and the current (state vectors) represented in Fig. 3.8 as follows:

$$\begin{bmatrix} V_1' \\ V_2' \\ I_1' \\ I_2' \end{bmatrix} = \mathbf{T} \cdot \begin{bmatrix} V_1 \\ V_2 \\ I_1 \\ I_2 \end{bmatrix}, \tag{3.15}$$

where V_j, I_j and V_j', I_j' (with $j = 1, 2$) represent the input and output voltages in the two microstrip lines in the proximity of the transistor, respectively, From Fig. 3.8 we can see that:

$$V_1' = V_1 = V_i, \qquad V_2' = V_2 = V_o \tag{3.16a}$$

$$I_1' = I_1 - I_i, \qquad I_2' = I_2 - I_o \tag{3.16b}$$

where V_i, I_i and V_o, I_o are the drain and gate voltages and currents, respectively, which are

connected by the admittance matrix $\mathbf{Y}_{\mathrm{F}}$ of the transistor as follows:

$$\begin{bmatrix} I_i \\ I_o \end{bmatrix} = \begin{bmatrix} Y_{11} & Y_{12} \\ Y_{21} & Y_{22} \end{bmatrix} \begin{bmatrix} V_i \\ V_o \end{bmatrix}. \tag{3.17}$$

Substituting Eq. 3.17 into the Eqs. 3.16, it follows that the ABCD matrix of the FET isolator can be determined by:

$$\begin{bmatrix} V_1' \\ V_2' \\ I_1' \\ I_2' \end{bmatrix} = \begin{bmatrix} 1 & 0 & 0 & 0 \\ 0 & 1 & 0 & 0 \\ -Y_{11} & -Y_{12} & 1 & 0 \\ -Y_{21} & -Y_{22} & 0 & 1 \end{bmatrix} \begin{bmatrix} V_1 \\ V_2 \\ I_1 \\ I_2 \end{bmatrix} \rightarrow \mathbf{f}' = \mathbf{T} \cdot \mathbf{f}. \tag{3.18}$$

To obtain the ABCD matrix for a single unit cell of the periodically loaded TL structure, it is supposed that the FET isolator is placed at the center of the unit cell [see Fig. 3.2]. In that case the ABCD matrix for a single cell $\mathbf{U}_c$ can be given by:

$$\mathbf{U}_c = e^{j\mathbf{M}_0 \frac{d}{2}} \cdot \mathbf{T} \cdot e^{j\mathbf{M}_0 \frac{d}{2}}. \tag{3.19}$$

In Eq. 3.19, $e^{j\mathbf{M}_0 \frac{d}{2}}$ is the ABCD matrix that describes the wave propagation in a section of the length of $d/2$ of the uncoupled TL.

$$e^{j\mathbf{M}_0 \frac{d}{2}} = \begin{bmatrix} \cos\left(\omega\sqrt{L_1 C_1}\frac{d}{2}\right) & 0 & -j\sqrt{\frac{L_1}{C_1}}\sin\left(\omega\sqrt{L_1 C_1}\frac{d}{2}\right) & 0 \\ 0 & \cos\left(\omega\sqrt{L_2 C_2}\frac{d}{2}\right) & 0 & -j\sqrt{\frac{L_2}{C_2}}\sin\left(\omega\sqrt{L_2 C_2}\frac{d}{2}\right) \\ -j\sqrt{\frac{C_1}{L_1}}\sin\left(\omega\sqrt{L_1 C_1}\frac{d}{2}\right) & 0 & \cos\left(\omega\sqrt{L_1 C_1}\frac{d}{2}\right) & 0 \\ 0 & -j\sqrt{\frac{C_2}{L_2}}\sin\left(\omega\sqrt{L_2 C_2}\frac{d}{2}\right) & 0 & \cos\left(\omega\sqrt{L_2 C_2}\frac{d}{2}\right) \end{bmatrix}. \tag{3.20}$$

Here $\mathbf{M}_0$ is the transfer matrix [see Eq. 3.8] of the TL without any capacitive coupling, i.e., considering $C_{12} = C_{21} = 0$. The transfer matrix for a finite structure with N unit cells is $[\mathbf{U}_c]^N$. Therefore, the state vectors at the input and output of a transmission with $l = Nd$ are connected by:

$$\mathbf{f}(y = Nd) = \left(e^{j\mathbf{M}_0 \frac{d}{2}} \cdot \mathbf{T} \cdot e^{j\mathbf{M}_0 \frac{d}{2}}\right)^N \cdot \mathbf{f}(y = 0). \tag{3.21}$$

Interestingly we see that the main difference between the continuous and discrete model is simply the transfer matrix associated with each problem, so that for the continuous problem it is given by $e^{j\mathbf{M}Nd}$, with $\mathbf{M}$ given by Eq. 3.8 and in the discrete model it is equal to $\left(e^{j\mathbf{M}_0 \frac{d}{2}} \cdot \mathbf{T} \cdot e^{j\mathbf{M}_0 \frac{d}{2}}\right)^N = [\mathbf{U}_c]^N$.

To verify the validity of the effective medium model introduced in the previous section, in what follows I also calculate the power distribution in the lines from the exact solution which

(discrete problem) which takes into account the periodicity of the structure. In this case, the eigenwaves are determined from the kernel of the matrix $\mathbf{U}_c$ and are also two eigenwaves, one ordinary and one extraordinary. For the sake of readability, their expressions are omitted in the text. Similar to the effective medium model, we consider that $V_1\,(y=0)=0$ at beginning of the lines, and also, for simplicity, we discard the effect of the dissipative elements of the FET isolators ($R_i=0$ and $R_{ds}=\infty$). In this model, we only compute the power at the periodicity nodes, i.e., at integer multiples of d. Fig. 3.9 depicts the total power transported in the lines for different values of the spacing d (between adjacent FET isolators) at the fixed frequency of $\omega/2\pi=5$GHz, calculated with the effective medium model and with the exact theoretical model.

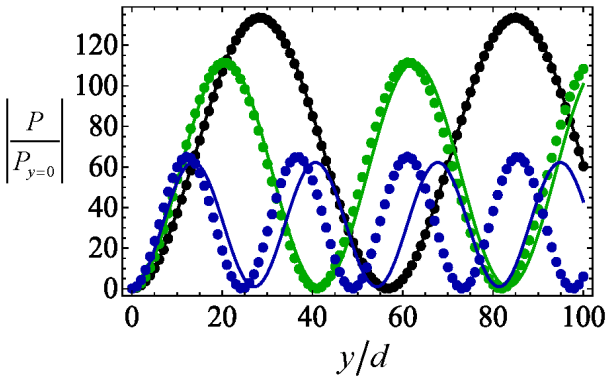

Figure 3.9: Power transported by the TL as a function of the propagation distance (normalized to the spacing d) at 5GHz. In the dotted black curve, we have $d_0=d/2.5=\lambda/30$, in the dotted green curve we have $d_1=d=\lambda/12$ and in the dotted blue curve, we have $d_2=3d=\lambda/4$, with λ being the wavelength in free-space $[\lambda=(2\pi c)/\omega]$ and $d=5$mm. The solid curves represent the effective medium (or continuous) model results and the discrete symbols represent the discrete (or periodic) model results.

These results depicted in Fig. 3.9 show a remarkable agreement between the two models (effective and periodic), especially for small periods, when compared to the free-space wavelength. When the period d becomes a significant fraction of the wavelength (blue curves in Fig. 3.9), this agreement starts to deteriorate and, as consequence, the effective medium approximation falls down. This is an expected behavior from the standard homogenization theory of metamaterials [16]. In metamaterials, the "inclusions" mimic the role of atoms and molecules of conventional materials, and, provided their size is much smaller than the wavelength of radiation, the metamaterial can be treated as a continuous medium described by some effective parameters. Similarly, the structure continuous model can describe accu-

rately the wave propagation in the metamaterial when the unit cell dimension d is on the order or smaller than $\lambda/10$ with $\lambda = (2\pi c)/\omega$.

3.3.3 Projected system

As previously mentioned, the 1D implementation of the MOSFET-MTM will be composed of two TL (microstrip lines), periodically loaded with FETs in a common-source configuration. In Fig. 3.10, it is depicted a representation of the idealized system wherein the gate of the transistors is connected to line 2 (bottom line) and the drain to line 1 (top line), with each line being terminated with a load (Z_1 and Z_2). I also considered the possibility of exciting the structure at both lines simultaneously, so that we have two voltages sources, $V_{g,1}$ and $V_{g,2}$ and their respective impedances, $Z_{g,1}$ and $Z_{g,2}$.

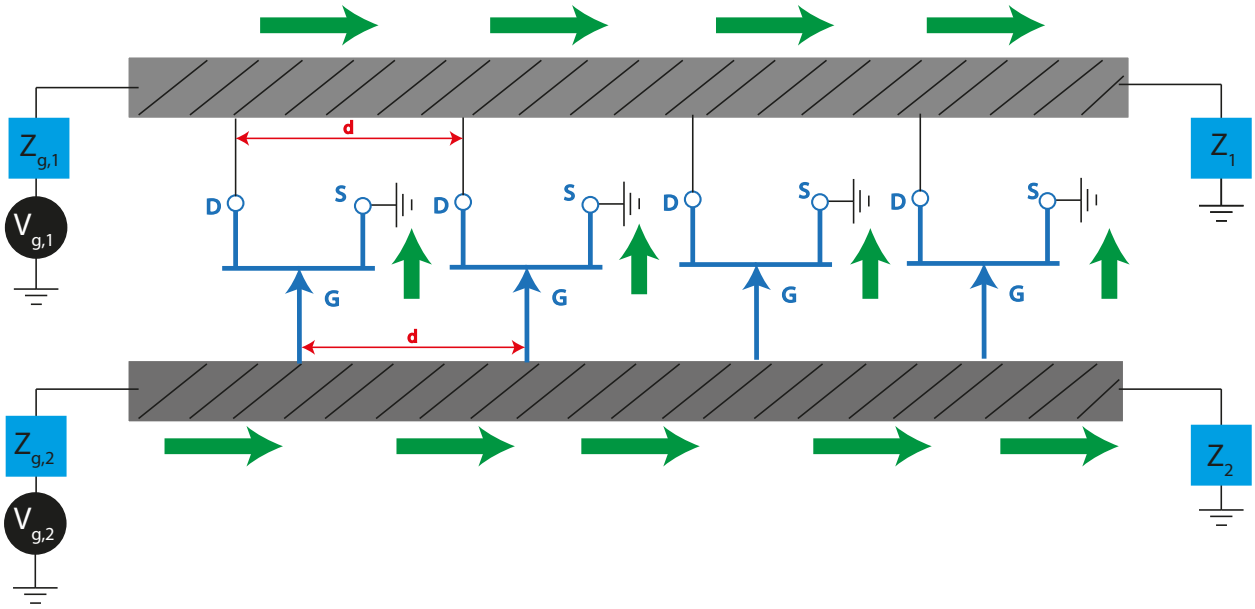

Figure 3.10: Sketch of the projected system, for a coupled TLs with $N = 4$ FETs.

In Fig. 3.10 it is depicted a coupled TL configuration with 4 FETs, but the system project may be extended to an arbitrary number of transistors. Despite being considered the possibility of exciting the structure from both sides, let us begin by focusing on a particular configuration wherein the coupled lines are excited on the left side of the gate line, and the output is on the right side of the drain line. As I showed in the previous section, such configuration gives rise to a power oscillation along the drain line, originating from the interaction between the ordinary and extraordinary waves propagating in line 1.

The prototype design also involved defining several structural parameters, such as frequency operation, line impedance, and spacing between FETs. Due to the limitations of

the oscilloscope that we will be using in the experimental characterization, the frequency of operation was restricted to around 2GHz. More precisely I considered $f = 1.8$GHz as the frequency of operation. While so far it was considered a fixed value of the effective permittivity of lines, in a realistic system this value will be heavily dependent on the width of the microstrip, the thickness, and permittivity of the substrate as shown in 3.11.

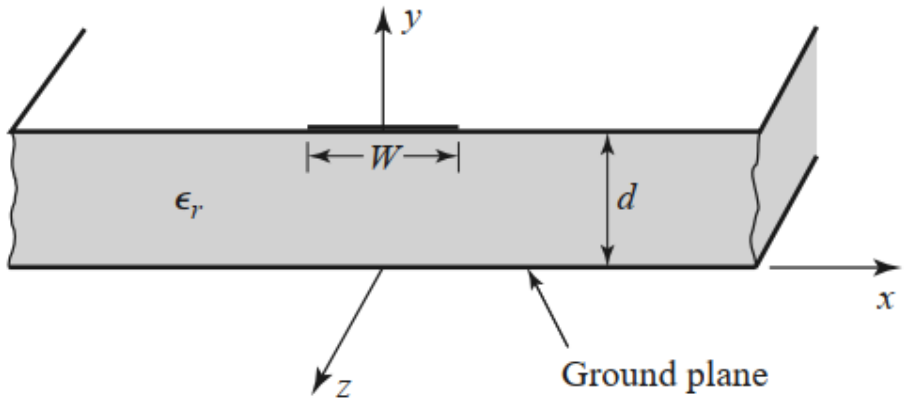

Figure 3.11: Geometry of a microstrip line. *Adapted from* [3].

The effective permittivity of the microstrip is given by:

$$\varepsilon_{ef} = \frac{\varepsilon_r + 1}{2} + \frac{\varepsilon_r - 1}{2} \frac{1}{\sqrt{1 + 12d/W}}, \tag{3.22}$$

with ε_r the relative permittivity of the substrate , d the thickness of the substrate and W the width of the microstrip line. Thus, the characteristic impedance of the lines can be given by:

$$Z_0 = \begin{cases} \frac{60}{\varepsilon_{ef}} \ln\left(\frac{8d}{W} + \frac{W}{4d}\right) & \text{for } W/d \leq 1 \\ \frac{120\pi}{\sqrt{\varepsilon_{ef}}[W/d + 1.393 + 0.667 \ln(W/d + 1.444)]} & \text{for } W/d \geq 1 \end{cases} \tag{3.23}$$

In this work I consider a FR4 substrate characterized by a relative permittivity $\varepsilon_r = 4.1$ and thickness $d = 0.8$mm. Since line 1 will be the line with the most power its impedance is set to 50Ω to ensure matching with the generator, whose standard impedance is 50Ω. Using the previous equations it follows that the effective permittivity of the line is $\varepsilon_{ef,1} = 3.14$ and its width is $W_1 = 1.83$mm. Conversely, I considered that the line 1 is characterized by a slightly different effective permittivity $\varepsilon_{ef,2} = 3.13$, for which the width of the line is $W_2 = 1.776$mm and the impedance is $Z_{02} = 51.1904\Omega$.

3.3.4 Theoretical system's characterization

In section 3.3.2 was studied the discrete model that determines the exact response of the system. In those studies it was considered that the initial condition was simply having $V_{g,1} = 0$V using a superposition of the system eigenstates, and that the system is infinite. In a more realistic problem it is challenging to excite the structure with its eigenstates and the most common way is by considering a generator as shown in Fig. 3.10. Moreover, the real configuration is not infinite but it is formed by N unit cells. To accomodate these changes in the theoretical model we assume that at the lines terminations ($y = l$) we have $I_1 = \frac{V_1}{Z_1}$, $I_2 = \frac{V_2}{Z_2}$, which give the state vector $\mathbf{f}(y = l) = A_1\hat{\mathbf{t}}_1 + A_2\hat{\mathbf{t}}_2$, with:

$$\hat{\mathbf{t}}_1 = \begin{bmatrix} 1 \\ 0 \\ 1/Z_1 \\ 0 \end{bmatrix}, \ \hat{\mathbf{t}}_2 = \begin{bmatrix} 0 \\ 1 \\ 0 \\ 1/Z_2 \end{bmatrix}$$

Here A_1 and A_2 are unknowns and represent the amplitudes of the voltages in each line. With this, and using simple mathematical manipulations in the transfer matrix it is easy to check that at the input of the system, the state vector verifies $\mathbf{f}(y = 0) = e^{-j\mathbf{M}l} \cdot \left(A_1\hat{\mathbf{t}}_1 + A_2\hat{\mathbf{t}}_2\right)$, which give:

$$\begin{bmatrix} V_1 \\ V_2 \\ I_1 \\ I_2 \end{bmatrix} = \begin{bmatrix} \hat{\mathbf{u}}_1 \cdot e^{-j\mathbf{M}I} \cdot \hat{\mathbf{t}}_1 & \hat{\mathbf{u}}_1 \cdot e^{-j\mathbf{M}I} \cdot \hat{\mathbf{t}}_2 \\ \hat{\mathbf{u}}_2 \cdot e^{-j\mathbf{M}I} \cdot \hat{\mathbf{t}}_1 & \hat{\mathbf{u}}_2 \cdot e^{-j\mathbf{M}I} \cdot \hat{\mathbf{t}}_2 \\ \hat{\mathbf{u}}_3 \cdot e^{-j\mathbf{M}I} \cdot \hat{\mathbf{t}}_1 & \hat{\mathbf{u}}_3 \cdot e^{-j\mathbf{M}I} \cdot \hat{\mathbf{t}}_2 \\ \hat{\mathbf{u}}_4 \cdot e^{-j\mathbf{M}I} \cdot \hat{\mathbf{t}}_1 & \hat{\mathbf{u}}_4 \cdot e^{-j\mathbf{M}I} \cdot \hat{\mathbf{t}}_2 \end{bmatrix} \begin{bmatrix} A_1 \\ A_2 \end{bmatrix} \tag{3.24}$$

Noting that $V_{g1} = Z_{g1}I_1 + V_1 = 0$ and $V_{g2} = Z_{g2}I_2 + V_2 = 1$, we obtain a linear system of 6 equations and 6 unknowns (which are V_1, V_2, I_1, I_2, A_1, and A_2), which can be numerically solve using Mathematica [17] to obtain the state vector at the input, and hence the voltages and currents at any point in the line, with the help of the ABCD matrix.

In Fig. 3.12 it is depicted the total power in the system (green curve), the power of line 1 (blue curve), and the power in line 2 (black curve) in function of the number of cells, for the discrete model, when line 2 is excited with 1V, i.e., $V_{g,2} = 1$V (with $d = 5$mm, $\varepsilon_{ef,1} = 3.14$, $\varepsilon_{ef,2} = 3.13$, $f = 5$GHz, and the system is composed by 100 cells), when the influence of the dissipative elements of the ideal FET is discarded. As seen, even when a finite structure and a more realistic excitation configuration is used, the structure still exhibits a *power beating* characteristic with the main contribution coming from line 1. Additionally, in Fig. 3.13 is

depicted the voltage and the current of the line (in function of the number of cells), which also reveal the beating effect of the traveling wave in the drain line.

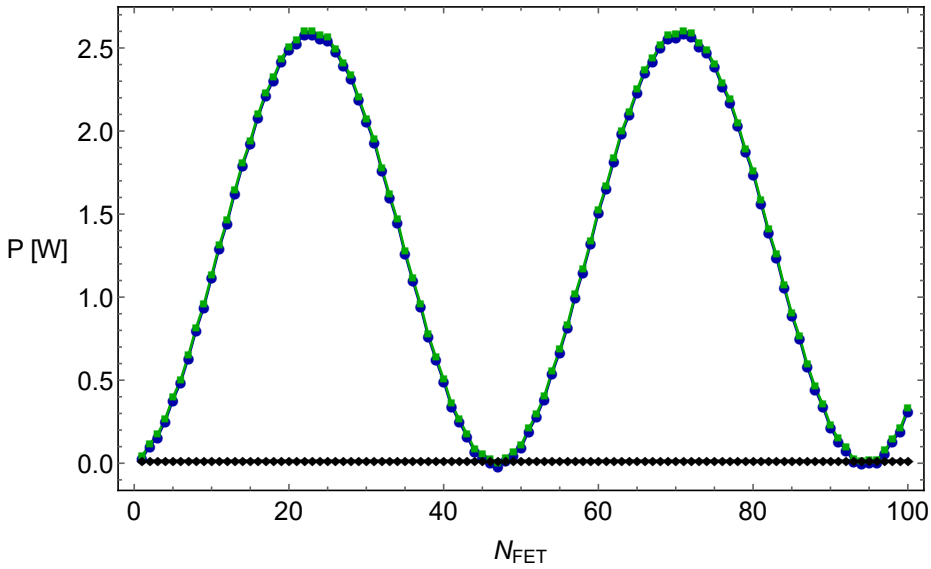

Figure 3.12: Power transported by the coupled lines as a function of the number of cells. The green curve represents the total power of the system, the blue curve represents the power of the traveling wave in line 1, and the black curve represents the power of the traveling wave in line 2.

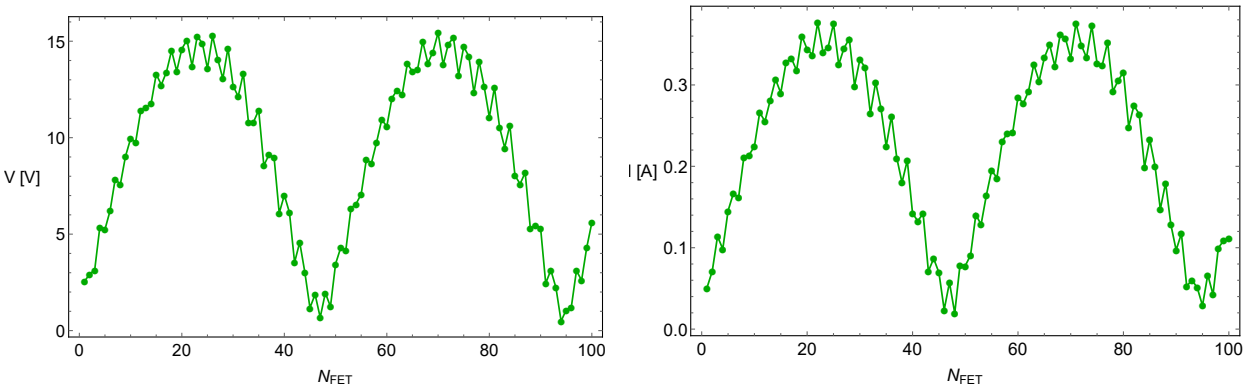

(a) (b)

Figure 3.13: a) Voltage in line 1, in function of the number of cells. b) Current in line 1, in function of the number of cells.

In Fig. 3.14 it is shown the power distribution in the lines when loss is considered in the system, particularly considering $R_i = 7\Omega$ and $R_{ds} = 400\Omega$. Similarly to the infinite configuration, the oscillations are damped. Interestingly, the maximum voltage gain in line 1 is 7V/V as shown in Fig. 3.15a.

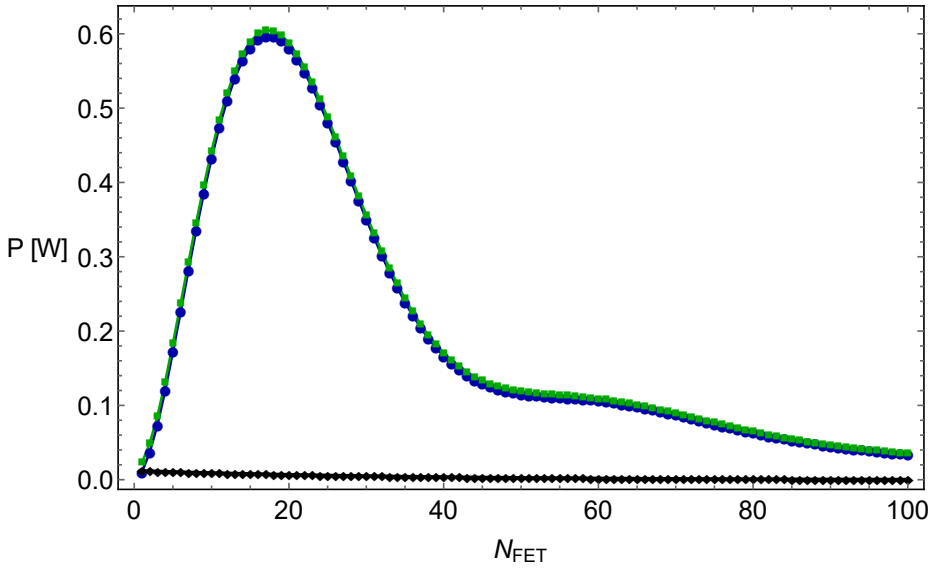

Figure 3.14: Power transported by the coupled lines as a function of the number of cells. The green curve represents the total power of the system, the blue curve represents the power of the traveling wave in line 1, and the black curve represents the power of the traveling wave in line 2.

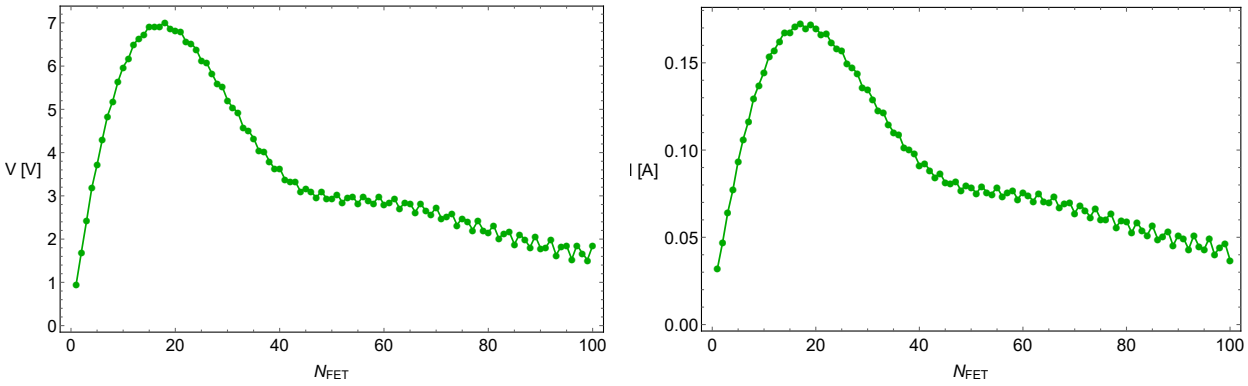

(a) (b)

Figure 3.15: a) Voltage in line 1, in function of the number of cells. b) Current in line 1, in function of the number of cells.

3.3.5 Characterization of the system with more realistic FETs

The system's analysis in the previous sections of this chapter treats the FETs as ideal isolators so that there is a unidirectional coupling between the gate and drain terminals. In particular, the gate-to-drain capacitance C_{gd} is neglected in the admittance matrix of the FET. However, in realistic devices C_{gd} can not be neglected, and one big consequence

of this is that the system will no longer have a unidirectional coupling [see Fig. 3.1]. So the objective of this section is to model the system with C_{gd} and other non-ideal elements (extrinsic or parasitic elements) of realistic transistors.

As shown in Fig. 3.16, the small-signal circuit of the FET can be divided into two parts: the intrinsic elements (elements inside the red box), which are dependent on the biasing of the FET, and the extrinsic elements (elements between the red and green boxes), which are the parasitic elements that came from the packaging.

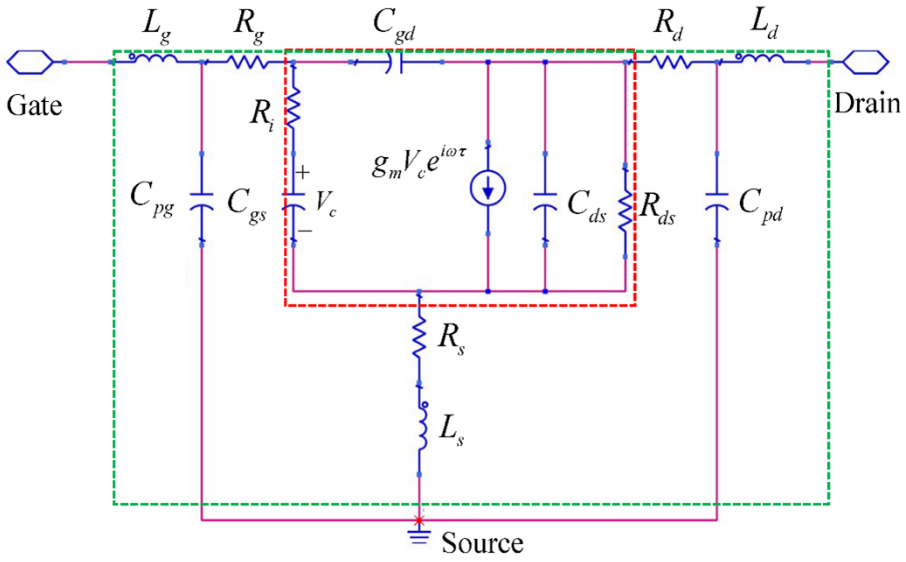

Figure 3.16: Complete small-signal equivalent circuit for a microwave FET in the common-source configuration. The intrinsic elements are enclosed in the red box and the extrinsic elements are enclosed in between the red and green boxes.

Thus, the admittance matrix $\mathbf{Y}_{\mathrm{F}}$ of the FET needs to be determined by taking into account all the elements depicted in Fig. 3.16. We start with the intrinsic response. A straightforward analysis of the circuit shows that the admittance matrix that describes the intrinsic response of the FET can be given by:

$$\mathbf{Y}_{\mathrm{F},int} = \begin{bmatrix} \frac{1}{R_{ds}} + j\omega C_{ds} + j\omega C_{gd} & \frac{g_m e^{-j\omega\tau}}{j\omega C_{gs} R_i + 1} - j\omega C_{gd} \\ -j\omega C_{gd} & \left(R_i + \frac{1}{j\omega C_{gs}}\right)^{-1} + j\omega C_{gd} \end{bmatrix}, \tag{3.25}$$

with τ the transit time required by carriers to travel from source to drain.

The entire admittance matrix $\mathbf{Y}_{\mathrm{F}}$ can be found starting from the intrinsic response through a series of matrix transformations [3], successively adding the parasitic elements to the overall response of the system [18]. This method consists of the following steps:

1. Transform the admittance matrix $\mathbf{Y}_{\mathrm{F},int}$ into an impedance matrix $\mathbf{Z}_{\mathrm{F},int}$. Then add

to $\mathbf{Z}_{\mathrm{F},int}$ the impedance matrix of the drain resistance and source parasitic elements:

$$\mathbf{Z}_1 = \mathbf{Z}_{\mathrm{F},int} + \begin{bmatrix} R_g + R_s + j\omega L_s & R_s + j\omega L_s \\ R_s + j\omega L_s & R_d + R_s + j\omega L_s \end{bmatrix}.$$

2. Transform the impedance matrix $\mathbf{Z}_1$ into an admittance matrix $\mathbf{Y}_1$. Then add to $\mathbf{Y}_1$ the admittance matrix of the drain and gate parasitic capacitances:

$$\mathbf{Y}_2 = \mathbf{Y}_1 + \begin{bmatrix} j\omega C_{pd} & 0 \\ 0 & j\omega C_{pg} \end{bmatrix}.$$

3. Transform the admittance matrix $\mathbf{Y}_2$ into an impedance matrix $\mathbf{Z}_2$. Then add to $\mathbf{Z}_2$ the impedance matrix of the drain and gate parasitic inductances:

$$\mathbf{Z}_{\mathrm{F}} = \mathbf{Z}_2 + \begin{bmatrix} j\omega L_d & 0 \\ 0 & j\omega L_g \end{bmatrix}.$$

4. Convert the impedance matrix $\mathbf{Z}_{\mathrm{F}}$ into th global matrix $\mathbf{Y}_{\mathrm{F}}$.

From hereon, in all the calculations it is considered the complete FET model and the ABCD matrix that takes into account the granularity (periodicity) of the system. It is also considered a comercially available MESFET [5] with the parameters listed in Table 3.2. With this, we can calculate the power flowing in the lines at integers multiples of d, the periodicity nodes of the structure.

Table 3.2: Parameters values of a commercially available MESFET [5].

Parameter	**Symbol**	**Value**
Source Resistance	R_s	0.8Ω
Source Inductance	L_s	0.04nH
Drain-Source Resistance	R_{ds}	100Ω
Drain-source Capacitance	C_{ds}	0.08pF
Drain Resistance	R_d	1Ω
Drain Pad Capacitance	C_{pd}	0.1pF
Drain inductance	L_d	0.28nH
Gate Bond Wire Inductance	L_g	0.1nH
Gate Pad Capacitance	C_{pg}	0.03pF
Gate Resistance	R_g	0.5Ω
Gate-Source Capacitance	C_{gs}	0.78pF
Channel Resistance	R_i	0.8Ω
Gate-Drain Capacitance	C_{gd}	0.1pF
Transconductance	g_m	120mS
Transit Time	τ	1ps

3.3.6 Numerical characterization of the system

To validate the theoretical results based on admittance and ABCD matrices and gain insight into the physical phenomena taking place, I simulated the structure in the commercially available software ADS by Pathwave [2]. This software allowed to do the implementation of the small-signal equivalent circuit of FET [see Fig. 3.16 and Table 3.2] [5]. The software allows to design a unit cell of the structure [see Fig. 3.17] that can be represented by a given symbol. Thus, it is possible to have a structure with multiple unit cells in a more compact form. In this cell I consider multiple input/output pins: pins P1 and P2 connect to the previous cell, pins P3 and P4 connect to the next cell, and pins P5 to P9 will be connected to probes to measure the voltage, current, and power at the end of each cell. In the unit cell there are also blocks that define the parameters in the TL, such as the impedance of the line, the spacing between the FET and the line termination (in the cell) and the effective permittivity of the line. Let me focus on the more realistic configuration discussed in the previous section. In that configuration, the incoming wave enters the structure on the left

side of the gate line (line 2) and the output is on the right side of the drain line (line 1), as depicted in Fig. 3.18.

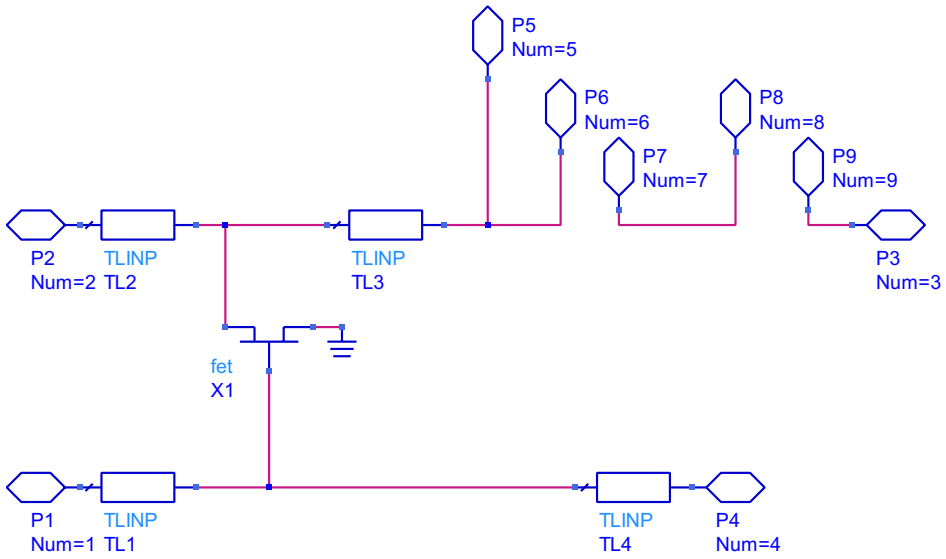

Figure 3.17: Screenshot of the schematic of a cell of the system, with the FET.

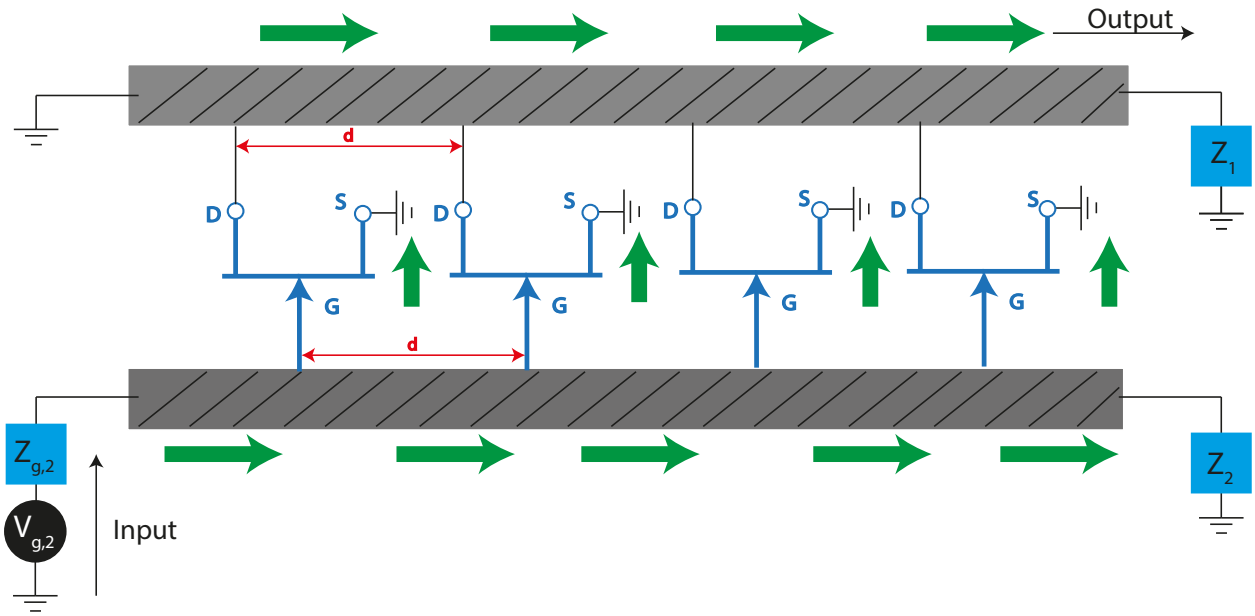

Figure 3.18: Schematic representation of the system in the left-side configuration.

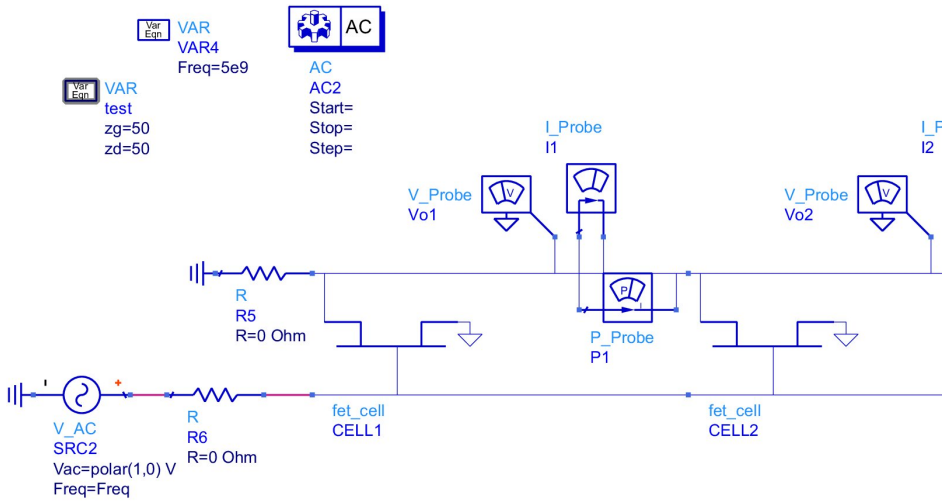

Figure 3.19: Screenshot of the beginning of the structure.

As we can see, at the beginning of the structure [see Fig. 3.19] we put an AC source voltage, that generates an AC voltage of 1V (polar) in line 2, while line 1 is connected to the ground. On the other hand, at the output of the system [see Fig. 3.20], both lines are terminated with an impedance of 50Ω and connected to the ground. Note that every cell of the structure is connected to three different probes of measurement (for voltage, current, and power measurements). This allows us to extract the information at the end of each cell.

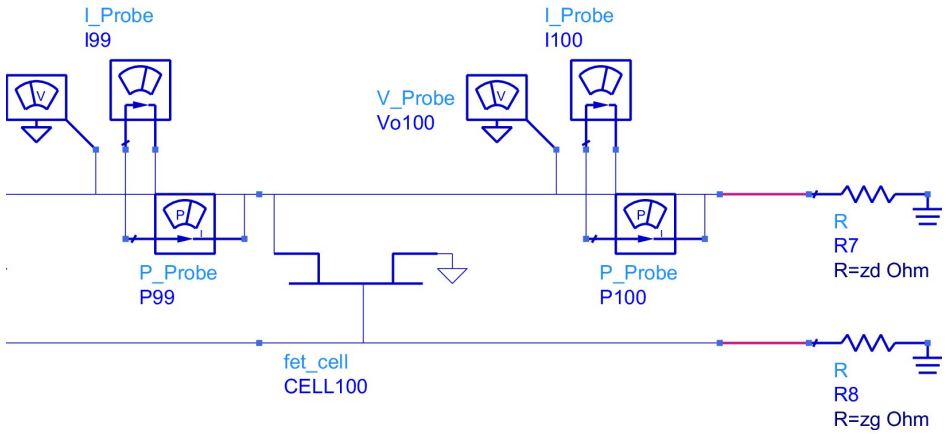

Figure 3.20: Capture of the end of the structure with 100 FET cells.

As previously mentioned, due to practical constrains the frequency of operation is limited to around 2GHz. In what follows I consider a structure operating at 2.2GHz and distance between successive FETs $d = 3cm$. Moreover, I also consider a smaller amount of FETs (15) so that the overall electric length of the structure $\omega \times d/c$ is nearly the same as in the previous example. In Fig. 3.21 is depicted the power measured (blue curve) and predicted in the theoretical model (green curve). The results calculated with the numerical simulation and

the theoretical model show perfect agreement and demonstrate that the proposed structure enables a *power beating* characteristic. Importantly, for $N = 15$ FETs the power in the end of the line (at $N = 15$) is almost null as the dissipative elements of the FETs absorb all the energy in the system. Remarkably, this phenomenon is very similar to the one of the MOSFET-MTM [1], and with this, one can validates that the 1D implementation based on TLs can emulate the behaviour of the MOSFET-MTM, even in a configuration with losses, and with a bidirectional coupling.

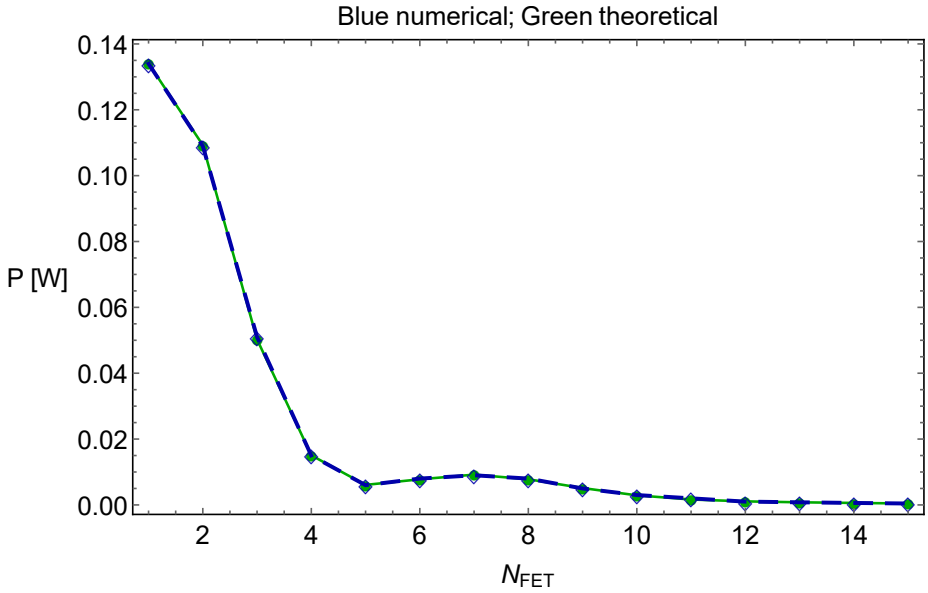

Figure 3.21: Power of the traveling wave in line 1, for the numerical model (blue curve) and for the theoretical model (green curve), with $f = 2.2$GHz, $d = 3$cm, $V_{g,1} = 0$V, $V_{g,2} = 1V$, $\varepsilon_{ef,1} = 3.14$, $\varepsilon_{ef,2} = 3.13$, $Z_{01} = 50\Omega$ and $Z_{02} = 51.1904\Omega$.

Additionally, I considered another configuration of the coupled TLs wherein the excitation signal is at the right-side of the gate line, as shown in Fig. 3.22. This configuration corresponds to a mirror symmetry of the structure depicted in Fig. 3.18.

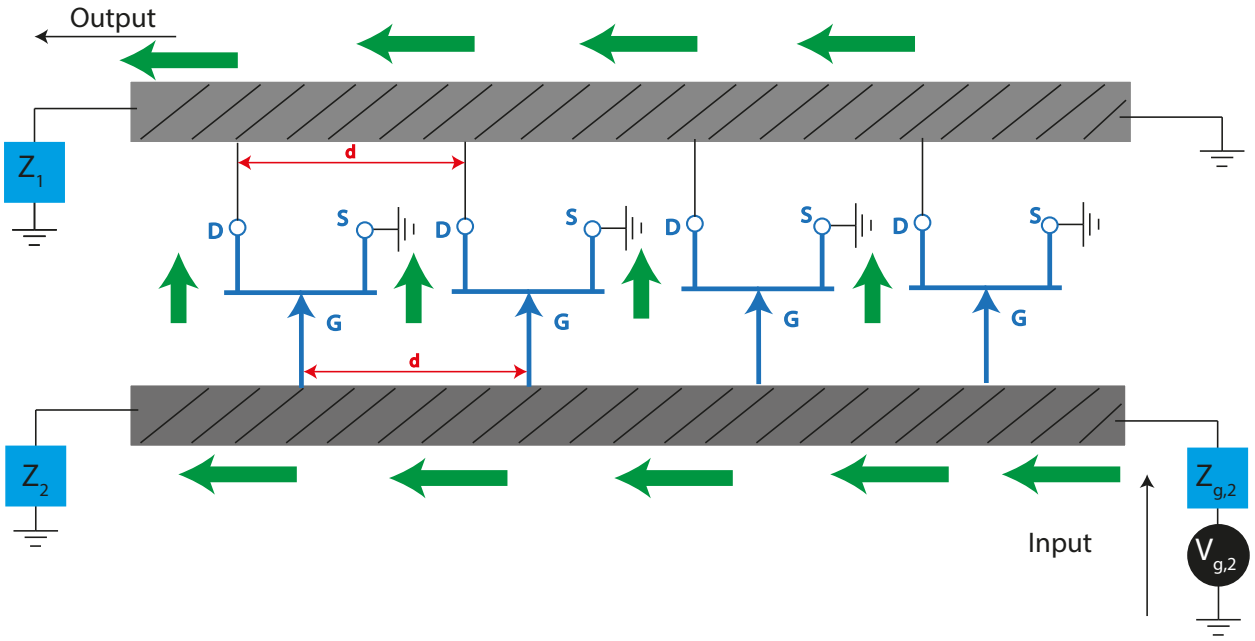

Figure 3.22: Schematic representation of the system in the right-side configuration.

The results of the power distribution in all space calculated using the simulator and the theoretical model are shown in Fig. 3.23. As seen, both results are overlapped and predict that in this case the power flow is along the negative $y-$direction. These results show us that this structure can be very flexible, because the incoming wave can be injected in any side of the structure and its behaviour will be the same, showing that despite the asymmetry of the TLs we have a symmetric response in the same TL.

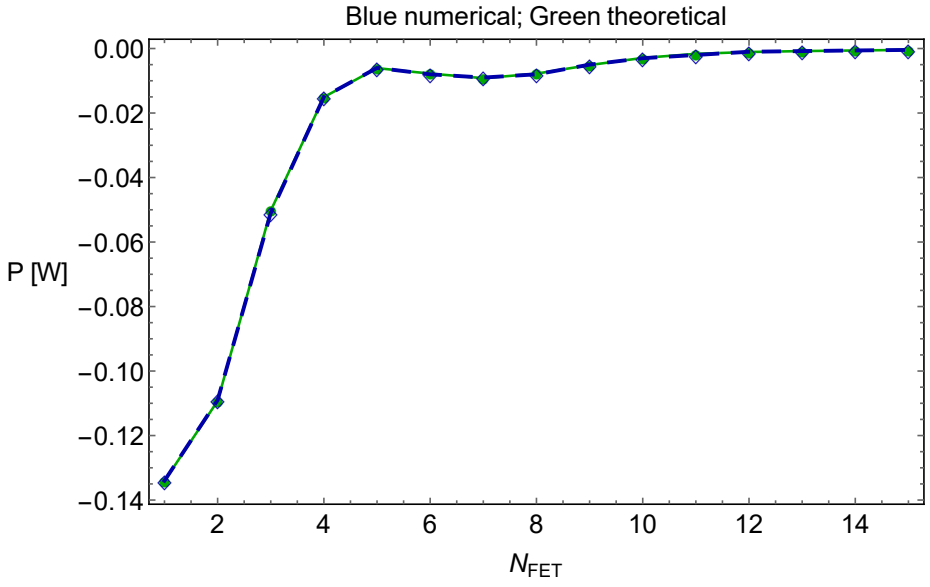

Figure 3.23: Power of the traveling wave in line 1 in the theoretical model (green curve) and in the numerical model (blue curve), with $f = 2.2$GHz, $d = 3$cm, $V_{g,1} = 0$V, $V_{g,2} = 1V$, $\varepsilon_{ef,1} = 3.14$, $\varepsilon_{ef,2} = 3.13$, $Z_{01} = 50\Omega$ and $Z_{02} = 51.1904\Omega$.

In Chapter 2 we have reported the possibility of taking advantage of the unique response of the MOSFET-MTM to realize an optical isolator. Here, we discuss the possibility of somehow mimic the MOSFET-MTM isolator with the proposed FET coupled TLs system. With this in mind, here we consider the system illustrated in Fig. 3.24. And we focus on a smaller structure with $N = 4$ FETs. Let's consider two different scenarios. In the first one the excitation is on the gate line and the measurements are done in the drain line [see Fig. 3.25]. In the other one the excitation is on the drain line is on the drain line and the measurements are made in the gate line [see Fig. 3.26].

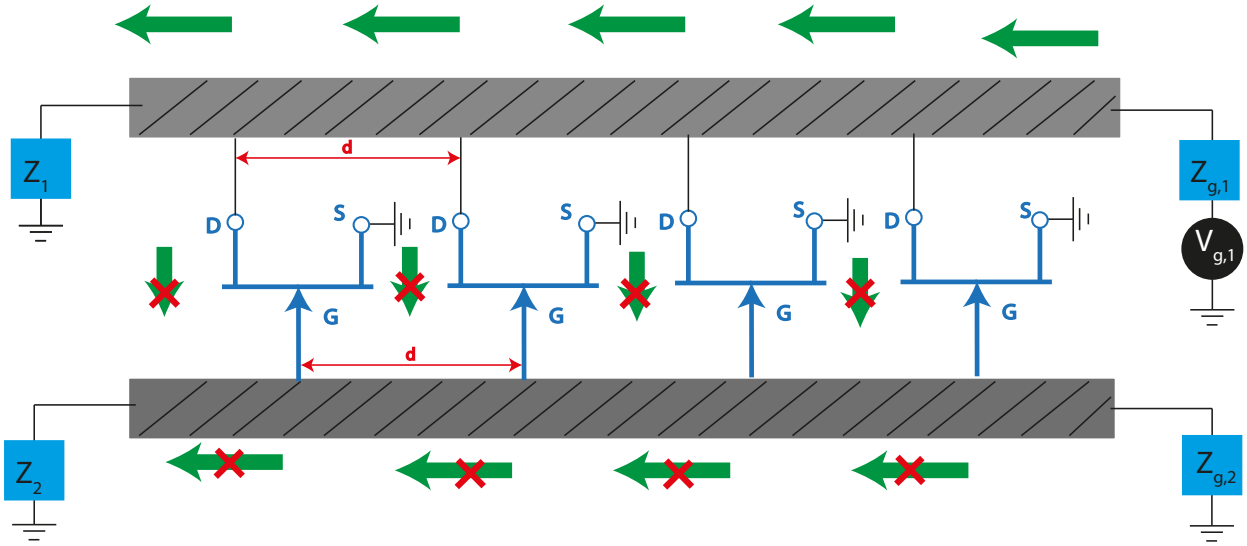

Figure 3.24: Representation of the structure as an isolator.

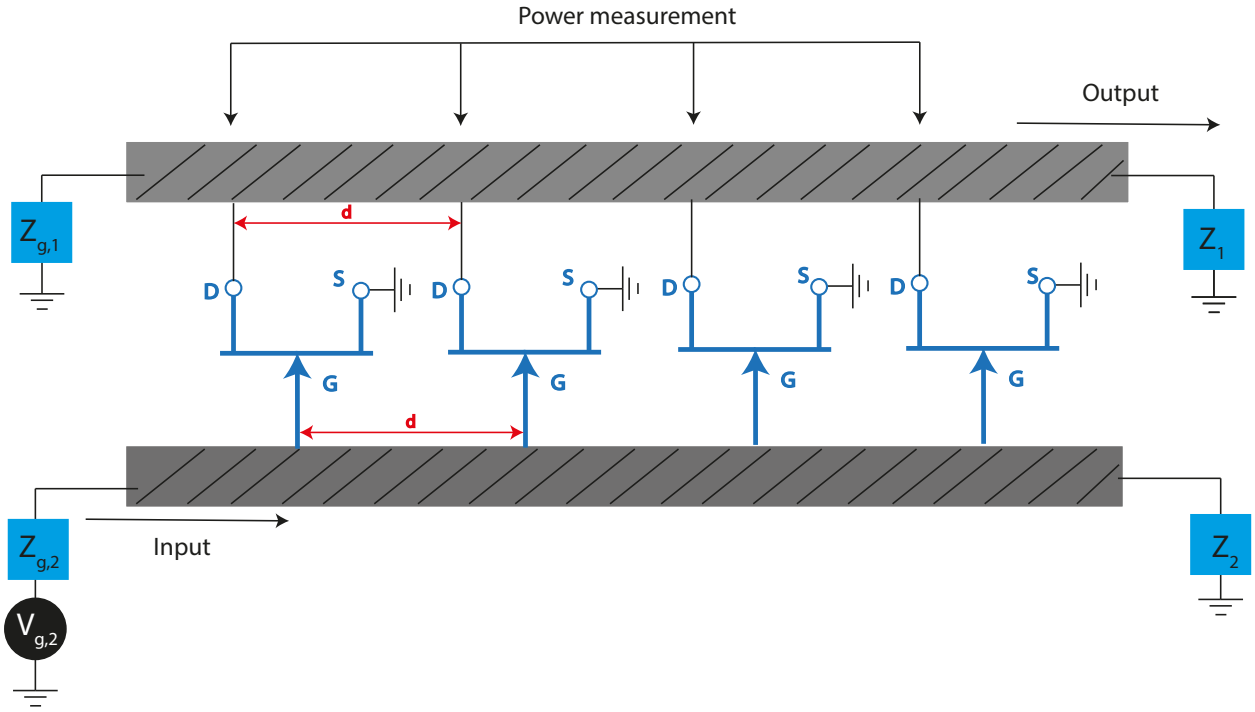

Figure 3.25: Representation of how the measurements of the isolator were done, with excitation on the gate line and measurements on the drain line.

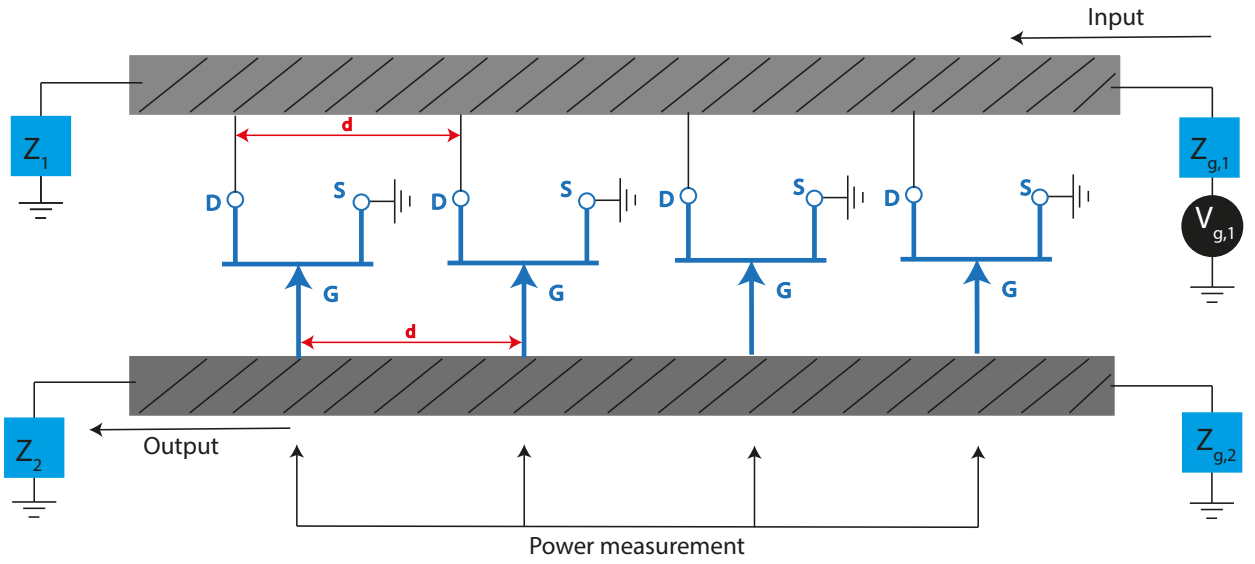

Figure 3.26: Representation of how the measurements of the isolator were done, with excitation on the drain line and measurements on the gate line.

As we can see from the results depicted in Figs. 3.27 the power in the drain line for a gate line excitation is much larger than the power in the gate line for a drain line excitation, with the latter being almost null. These results show in a definite manner that the proposed 1D analog of the MOSFET-MTM can also operate as an effective isolator. It is also important to emphasize the discrepancies between the numerical an theoretical results in Fig. 3.27b

are only due to numerical errors in the numerical implementation of the theoretical model in Wolfram Mathematica software [17], particularly because this model uses the matrix power.

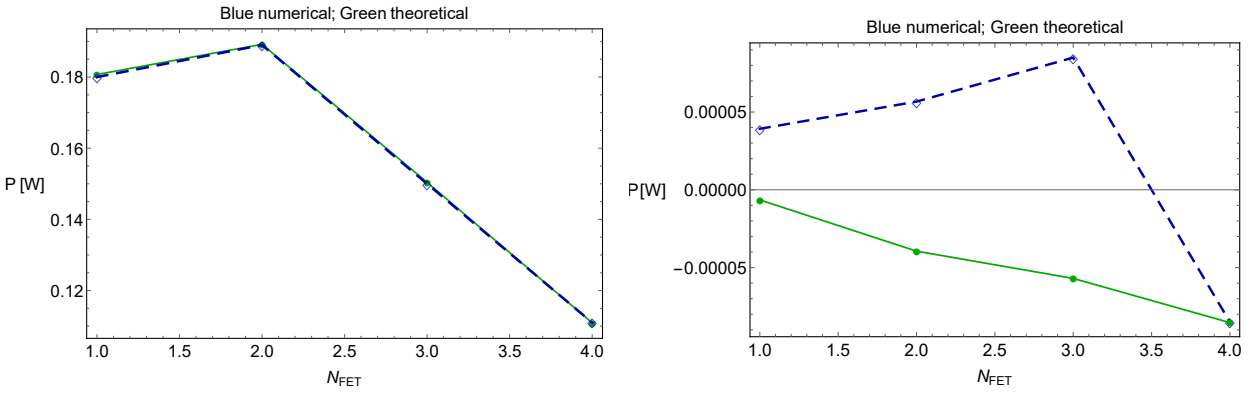

(a) (b)

Figure 3.27: a) Power measured in the configuration represented in Fig. 3.25, with $f = 2.2\text{GHz}$, $d = 3\text{cm}$, $V_{g,1} = 0\text{V}$, $V_{g,2} = 1V$, $\varepsilon_{ef,1} = 3.14$, $\varepsilon_{ef,2} = 3.13$, $Z_{01} = 50\Omega$ and $Z_{02} = 51.1904\Omega$. b) Power measured in the configuration represented in Fig. 3.26, with $f = 2.2\text{GHz}$, $d = 3\text{cm}$, $V_{g,1} = 1\text{V}$, $V_{g,2} = 0V$, $\varepsilon_{ef,1} = 3.14$, $\varepsilon_{ef,2} = 3.13$, $Z_{01} = 50\Omega$ and $Z_{02} = 51.1904\Omega$.

3.3.7 Prototype and experimental characterization

Based on the studies made on the previous sections (numerical and theoretical) it is intended to fabricate two prototypes: one with $N = 4$ FETs to demonstrate the isolator, and another with $N = 15$ FETs to demonstrate the *power beating*. The prototype will be fabricated using standard printed circuit techniques. The printed circuit schematics will be drawn in the commercially available software EAGLE EDA [4]. A first schematic of a $N = 4$ FETs prototype drawn in the EAGLE is shown in Fig. 3.28. In the design of the schematic of the circuits to be fabricated, we need to take into account important details that were not considered so far. In particular, we need to include the DC biasing circuit of the FETs.

As for the components, in the prototype, are present the FETs MwT-A973 by MwT Inc. [5], the SMA connectors [19], and the capacitances required to filter the DC component of the signal to prevent it from entering the signal generator. The SMA connectors must be at the terminations of each line, so it is required four of them, one for each line termination. By analyzing the datasheet of the component [19], it is possible to see that it is ideal for PCB boards with 0.8mm and that it has an impedance of 50Ω, which is in agreement with all the simulations previously made. As for the capacitances, it is only required that they

had a value of at least 0.1pF, thus it was designed the system with capacitances of 15pF [20]. Additionally, the structure requires two types of loads that need to be put in the terminations of each line, which will be connected to the SMA connectors, these are 50Ω loads [21] and short-circuit loads [22].

Another thing that must be considered is to first build a smaller prototype, that will validate theoretical and numerical models of the system. This smaller prototype has only four FET cells, as it is depicted in Fig. 3.28

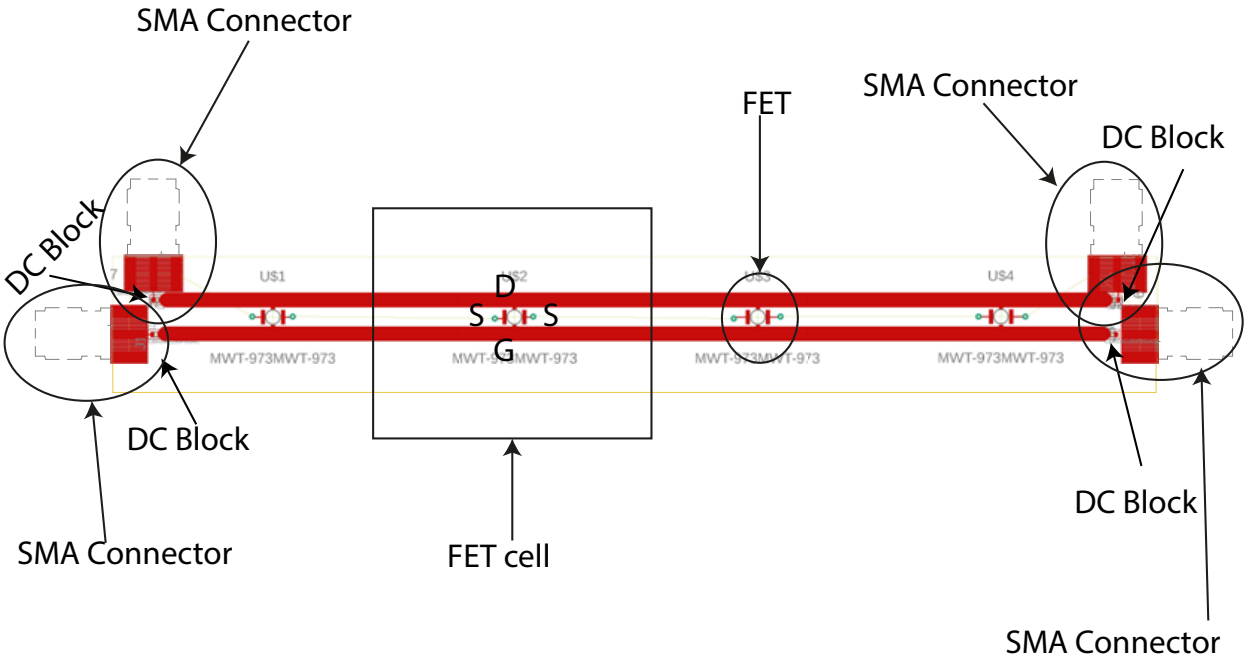

Figure 3.28: Schematic of the smaller prototype designed in the EAGLE [4] software, with the components listed. Below This structure there is a ground plane, which the GND pins of the SMA connectors and the sources of the FETs are connect.

3.3.8 Results and discussions

Remarkably, in the previous sections I was able to demonstrate and validate that it is possible to do a realistic implementation of the 1D analogue MOSFET-MTM, based on coupled TL, both theoretically and numerically. Even when all the dissipative elements that may be part of a system like this are taken into account, this structure exhibits strong nonreciprocal and non-Hermitian response. Also, it is shown the unique wave phenomena of the *power beating*. Additionally, I was able to validate that this same structure may also behave as an isolator.

I was also proposed and designed a 1D prototype of the coupled lines based on PCB techniques and commercially available SMD elements. Due to the shortage of time and the

fact of the company responsible for producing the prototype was not able to ensure a timely delivery of the prototype, it was not possible to complete the experimental characterization of the proposed prototype.

4 Conclusions

In this dissertation, I have studied and characterized the wave propagation in a system formed by two microstrip TLs periodically loaded with FET isolators, which can be regarded as 1D analog of the MOSFET-MTM introduced in [1]. The wave propagation in the asymmetrically coupled TLs was first theoretically studied using standard circuit analysis techniques, such as admittance and ABCD matrices. Two different theoretical methods were used: (i) an effective medium (or continuous) model where it is assumed that the FETs parameters are distributed along the lines; (ii) a more realistic discrete model where the periodic loading with FETs of the lines is taken into account. It was shown that for subwavelength distances between adjacent FETs, the continuous model agrees well with the distributed model. In addiction, both theoretical models were validated against numerical simulations done in ADS [2].

It was shown that the coupled TL system supports the propagation of two different travelling waves: an ordinary and an extraordinary waves. Moreover, it was shown that each line is associated with a certain wave polarization, and that the two wave polarizations are coupled through the FETs isolators. The theoretical and numerical results clearly demonstrated that the TL analog imitates very faithfully the behaviour of the idealized MOSFET-MTM. In particular, it was demonstrated theoretically and numerically that the FET-coupled TLs system enables optical isolation and a *power beating* effect where it oscillates between gain and loss regimes as the wave propagates, analogous to what is provided by the MOSFET-MTM [1]. Finally, a microwave prototype will be soon fabricated using standard printed circuit techniques and then experimentally characterized using a VNA and digital oscilloscope.

5 Bibliography

[1] S. Lannebère, D. E. Fernandes, T. A. Morgado, and M. G. Silveirinha, "Nonreciprocal and non-hermitian material response inspired by semiconductor transistors," *Physical Review Letters*, vol. 128, no. 1, p. 013902, 2022.

[2] Keysight, "Pathwave advanced design system." `https://www.keysight.com/zz/en/products/software/pathwave-design-software/pathwave-advanced-design-system.html`.

[3] D. M. Pozar, *Microwave Engineering*. John Wiley & Sons, 4th ed., 2011.

[4] Autodesk, "Eagle." `https://www.autodesk.com/products/eagle/overview?term=1-YEAR&tab=subscription`.

[5] M. Inc., "Gaas fet mwt-9/a9." `https://www.mwtinc.com/wp-content/uploads/2017/01/mwt-9_A9.pdf`.

[6] E. Galiffi, R. Tirole, S. Yin, H. Li, S. Vezzoli, P. A. Huidobro, M. G. Silveirinha, R. Sapienza, A. Alù, and J. Pendry, "Photonics of time-varying media," *Advanced Photonics*, vol. 4, no. 1, p. 014002, 2022.

[7] D. L. Sounas and A. Alù, "Non-reciprocal photonics based on time modulation," *Nature Photonics*, vol. 11, no. 12, pp. 774–783, 2017.

[8] T. Kodera, D. L. Sounas, and C. Caloz, "Artificial faraday rotation using a ring metamaterial structure without static magnetic field," *Applied Physics Letters*, vol. 99, no. 3, p. 031114, 2011.

[9] T. A. Morgado and M. G. Silveirinha, "Drift-induced unidirectional graphene plasmons," *ACS Photonics*, vol. 5, no. 11, pp. 4253–4258, 2018.

[10] A. M. Mahmoud, A. R. Davoyan, and N. Engheta, "All-passive nonreciprocal metastructure," *Nature communications*, vol. 6, no. 1, pp. 1–7, 2015.

[11] D. E. Fernandes and M. G. Silveirinha, "Asymmetric transmission and isolation in nonlinear devices: Why they are different," *IEEE Antennas and Wireless Propagation Letters*, vol. 17, no. 11, pp. 1953–1957, 2018.

[12] L. Feng, R. Elganainy, and L. Ge, "Non-hermitian photonics based on parity–time symmetry," *Nature Photonics*, vol. 11, pp. 752–762, 11 2017.

[13] R. Elganainy, M. Khajavikhan, D. Christodoulides, and S. Ozdemir, "The dawn of non-hermitian optics," *Communications Physics*, vol. 2, 12 2019.

[14] D. R. Barton, H. Alaeian, M. Lawrence, and J. Dionne, "Broadband and wide-angle nonreciprocity with a non-hermitian metamaterial," *Phys. Rev. B*, vol. 97, p. 045432, Jan 2018.

[15] S. Buddhiraju, A. Song, G. T. Papadakis, and S. Fan, "Nonreciprocal metamaterial obeying time-reversal symmetry," *Phys. Rev. Lett.*, vol. 124, p. 257403, Jun 2020.

[16] M. G. Silveirinha, "Nonlocal homogenization theory of structured materials," in *Theory and Phenomena of Artificial Materials* (F. Capolino, ed.), CRC Press, Oct. 2009.

[17] Wolfram, "Mathematica." `https://www.wolfram.com/mathematica/`.

[18] G. Dambrine, A. Cappy, F. Heliodore, and E. Playez, "A new method for determining the fet small-signal equivalent circuit," *IEEE Transactions on Microwave Theory and Techniques*, vol. 36, no. 7, pp. 1151–1159, 1988.

[19] M. PRO, "Mp-19-70-4-tgg." `https://www.farnell.com/datasheets/3204418.pdf`.

[20] KEMET, "Cbr04c150f5gac." `https://connect.kemet.com:7667/gateway/IntelliData-ComponentDocumentation/1.0/download/datasheet/CBR04C150F5GAC`.

[21] A. RF, "132360." `https://pt.farnell.com/amphenol-connex/132360/rf-coaxial-sma-plug-50ohm/dp/2112480?MER=sy-me-pd-mi-alte`.

[22] A. RF, "132331." `https://4donline.ihs.com/images/VipMasterIC/IC/AMPH/AMPHS07097/AMPHS07097-1.pdf?hkey=52A5661711E402568146F3353EA87419`.